



**FP7-600716**

**Whole-Body Compliant Dynamical Contacts in Cognitive Humanoids**

**Year 4**  
**Fourth year project objectives report**

<b>Editor(s)</b>	CoDyCo Consortium
<b>Responsible Partner</b>	IIT
<b>Affiliations</b>	IIT, TUD, UPMC, UB, JSI.
<b>Status-Version:</b>	Draft-1.0
<b>Date:</b>	Apr. 28, 2017
<b>EC Distribution:</b>	Consortium
<b>Project Number:</b>	600716
<b>Project Title:</b>	Whole-Body Compliant Dynamical Contacts in Cognitive Humanoids
<b>Title of Report:</b>	Fourth year project objectives report
<b>Date of delivery to the EC:</b>	28/04/2017
<b>Workpackage responsible for the Report</b>	All work packages
<b>Editor(s):</b>	Francesco Nori, Vincent Padois, Jan Peters, Jan Babic, Michael Mistry, Serena Ivaldi
<b>Contributor(s):</b>	Entire CoDyCo consortium
<b>Reviewer(s):</b>	reviewers
<b>Approved by:</b>	All Partners

## Table of Contents

3.2 Project objectives for the period . . . . .	6
3.2.1 Overview . . . . .	6
3.2.1.1 WP1: toolbox for computing and controlling dynamics of whole-body movements with contacts (UB) . . . . .	6
3.2.1.2 WP2: understanding and modelling human whole-body behaviours in physical interaction (JSI) . . . . .	6
3.2.1.3 WP3: control and optimization of whole-body motion in contact (UPMC) . . . . .	6
3.2.1.4 WP4: adaptation, Generalization and Improvement of Compliant Control and Tasks with Contacts (TUD) . . . . .	7
3.2.1.5 WP5: systems integration, standardization and evaluation on the iCub robot (IIT) . . . . .	7
3.2.1.6 WP6: management (IIT) . . . . .	7
3.2.1.7 WP7: dissemination and Exploitation (IIT) . . . . .	7
3.3 Work progress and achievements during the period . . . . .	7
3.3.1 Progress overview and contribution to the research field . . . . .	7
3.3.2 Work packages progress . . . . .	7
3.3.2.1 Work package 1 progress . . . . .	10
3.3.2.2 Work package 2 progress . . . . .	14
3.3.2.3 Work package 3 progress . . . . .	34
3.3.2.3.1 Solving the local control problem (T3.3) (IIT: xxPM, UPMC: 3PM) . . . . .	34
3.3.2.3.2 Bootstrapping and validating the control approach in rigid world and compliant cases (T3.4) (TUD: 3.6PM, UPMC: 5.51PM, UB: xxPM, JSI: 1 PM, INRIA: 1.98PM) . . . . .	35
3.3.2.3.3 Extra results in WP2/WP3: UPMC and JSI collaboration . . . . .	39
3.3.2.3.4 Deviations from workplan . . . . .	39
3.3.2.3.5 Resources . . . . .	39
3.3.2.4 Work package 4 progress . . . . .	39
3.3.2.4.1 Learning the Prioritization of Tasks (T4.4) (TUD: 4PM) . . . . .	39
3.3.2.4.2 Learning the Prioritization of Tasks (T4.4) (INRIA: 4.02PM) . . . . .	40
3.3.2.4.3 Task compatibility optimization (T4.4) (UPMC: 1.87PM) . . . . .	40
3.3.2.5 Work package 5 progress . . . . .	41
3.3.2.5.1 Scenario 4: learning how to stand up with the help of a human caregiver (T5.4) . . . . .	41
3.3.2.5.2 Deviations from workplan . . . . .	42
3.3.2.6 Work package 6 progress . . . . .	45
3.3.2.6.1 Administrative coordination (T6.1) . . . . .	45

3.3.2.6.2	Software repository implementation (T6.2) . . . . .	45
3.3.2.7	Work package 7 progress . . . . .	46
3.3.2.7.1	Dissemination activities towards academia, industry, and other users (T7.1) . . . . .	46
3.3.2.7.2	Exploitation plan (T7.2) . . . . .	46
3.3.2.7.3	Management of IPR (T7.3) . . . . .	46
3.3.2.7.4	Dissemination of a database of human motion with contacts (T7.4) . . . . .	46
3.4	Deliverables and milestones tables . . . . .	46
3.4.1	Deliverables (excluding the periodic and final reports) . . . . .	46
3.4.2	Milestones . . . . .	46

## Index of Figures

1	Whole-body Interface software architecture . . . . .	12
2	Human interacting with the iCub Robot. The BERDY algorithm can be used to estimate online both the dynamics of the robot and of a human. . . . .	13
3	Feasible CoM acceleration polygons due to torque limits and CoM dynamic manipulability ellipses for four different planar robots. The black polygons and red ellipses are for constrained end-effectors whereas the grey polygons and blue ellipses are for unconstrained robots at the same configuration. The gravity and velocity are assumed to be zero ( $\ddot{c}_{vg} = 0$ ). . . . .	15
4	CoM dynamic manipulability ellipses for a five-link planar robot in different velocities. The robot's configuration is shown on the bottom left corner. Straight lines show the friction cone of the contact force. . . . .	16
5	CoM dynamic manipulability ellipses and feasible CoM acceleration polygons due to torque limits and unilateral constraints of a four-link robot with two contact points in different velocities. Straight lines show the friction cone of the total force. . . . .	17
6	CoM dynamic manipulability ellipses with different weighting matrices for a planar five-link robot in two configurations. Green areas show feasible CoM accelerations due to torque limits. Blue and red areas show achievable CoM accelerations with unit weighted norms of joint accelerations. . . . .	20
7	Four different force dynamics are applied. [1] Linear, [2] Non-linear (quadratic), [3] Non-linear (concave), and [4] Half-linear. The [1],[2],[3] are the same force at the end position (e.g., $z=-0.12$ ), and [2] and [4] are the same force at the half position (e.g., $z=-0.06$ ). . . . .	21
8	The test trial performances averaged across 18 participants.(a) the end-effector position at the test half-position trial and (b) the applied force at the test half-force trial. The red lines indicate the ideal values based on the dynamics (see Figure 1). . . . .	22
9	(a) Learning performance of the 18 participants along with the standard error. A big variation in the learning performance of the three different forces is observed within the initial 10 trials. (b) Average time taken by the 18 participants to reach the target with the three different forces. . . . .	23

- 10 Multifinger contact effects on (A, above) 2-interval force choice (2-IFC) and (B, below) absolute magnitude estimates (AME) measures of roughness perception. In both tasks participants actively explored a target and distractor surface simultaneously using 2 digits; the digits were either on one hand or two hands, expected to result in more or less crosstalk. In the 2-IFC task (A), participants identified the rougher of a pair of target stimuli and were instructed to ignore the distracter. The red circles and line indicate group (N=12) average performance when the fine surfaced target was paired with various coarse distractor surfaces; a fine distractor depresses accuracy more than a coarse distractor. The blue circles and line show behaviour with the coarse target; a coarse distractor depresses accuracy more than does a fine one. The bar graph summarising mean slope across participants shows the distraction effect is greater in the one hand condition. In the AME task (B), participants rated the roughness of target surfaces while instructed to ignore the simultaneously touched distracter. The graph at the top of figure 1b shows mean ratings for each target surface. The blue crosses and squares show mean ratings for each target surface with a coarse distractor surface. Mean ratings with a fine distractor surface are shown in red. It can be seen that a coarse distracter results in higher roughness ratings than does a fine distracter. As with 2-IFC, the distracter effects are greater with the distracter on the same hand as the target. . . . . 24
- 11 Activations during passive touch. The three panels indicate sagittal, coronal and horizontal planar sections of the brain with multisensory activations for a tactile discrimination task contrasting coarse and fine texture perception under moving and static touch conditions. Regions of interest shown with coloured blobs, were more activated for moving (vs static) touch, including auditory cortex (TE1.0). The stimuli were applied to the right index finger of passive participants, N=13; Light blue: BA1, Green: OP1, Red: OP3, Yellow: OP4, Blue: TE1.0 . . . . . 25
- 12 Joint lifting action. The participants worked in pairs to lift a bar to a target height. The weight at the centre of the bar (either 200g or 700g) was known to one, both or neither participant in pair. The force with which the participants held the bar in anticipation of a lift in the different knowledge conditions is shown along with on SE of the mean. . . . . 26
- 13 The spring model in the Haptic API is used to emulate the performance of a robot model (mass) and the human applies the force along the x and z directions similar to a planar movement which is visualized using the model in real time. . . . . 27
- 14 External forces applied by the participant along the x and z axis are measured using the Haptic Master device. . . . . 28
- 15 Resulting torque applied to the planar robot model, The torque performance varied depending on the External force applied by the user and the controller output. . . . . 28

16	Experimental setup. The subject is standing on a movable platform and a lighted area appears on the floor in front of his leg, serving as a stepping cue and target. . . . .	30
17	Stepping errors. Error bars indicate standard deviation. Statistics are given in the text. . . . .	30
18	Step onset time (time from the cue to step to foot lift-off). Error bars indicate standard deviation. Statistics are given in the text. . . . .	31
19	Step execution time (time from step onset to landing). Error bars indicate standard deviation. Statistics are given in the text. . . . .	32
20	SD of the COM displacement (mm). . . . .	33
21	Range of the COM displacement (mm). . . . .	33
22	iCub leg setup used for the experiments. The red circles identify the hip and knee joints, while the white marks indicate joint limits. The green arrow shows the external force applied during experiments. . . . .	35
23	KUKA LWR IV arms with two soft surfaces used in our experiments. . . . .	36
24	A modern control hierarchy for highly redundant robotic systems, e.g. humanoid robots. At the lowest level is whole-body control, which determines the torques needed to accomplish a set of tasks. At the intermediate level, these tasks are controlled by the servoing/MPC level where task trajectory errors are compensated using state feedback. Finally the task trajectories are provided by high-level planning, which is usually a combination of operator expertise and automated planning. Each of these levels operates independently from one another and a feedback mechanism is needed to measure and compensate for tasks which are not executed as planned. This is the role of the Task Compatibility Optimization loop proposed in this work. . . . .	38
25	CoM dynamic manipulability with respect to arm configuration. . . . .	42
26	CoM dynamic manipulability with respect to shoulder pitch angle. . . . .	43
27	CoM dynamic manipulability with respect to elbow angle. . . . .	43
28	iCub in optimum sitting configuration. . . . .	44
29	iCub in near-optimum sitting configuration. . . . .	44

## 3.2 Project objectives for the period

### 3.2.1 Overview

The specificity of CoDyCo relies on the fact that the progress beyond the state of the art is guided by the yearly implementation on the iCub humanoid. Within this context, iCub is a peculiar platform being the only humanoid integrating whole-body distributed force and tactile sensors. In this sense CoDyCo fourth year specific objectives were to design and implement the control of whole-body posture during physical human robot interaction. Other long term objectives involve setting up the necessary infrastructure (human experimental protocols, software infrastructure, learning and control specifications) for leveraging the activities in previous years.

Task	IIT	TUD	UPMC	UB	JSI	INRIA	
WP1	0.00	1.00	-	2.18	2.00	2.96	8.14
WP2	-	3	1.20	13.88	21.69	0.52	38.29
WP3	-	3.6	8.79	1.63	2.00	4.03	26.10
WP4	9.79	4	0.74	1.68	3.00	3.30	30.51
WP5	13.06	2	0.14	1.44	-	0.52	17.16
WP6	1.51	0	0.19	-	0.44	-	3.14
WP7	1.00	1	0.11	-	-	-	1.11
	25.36	14.6	11.17	20.81	29.13	11.33	<b>123.45</b>

**3.2.1.1 WP1: toolbox for computing and controlling dynamics of whole-body movements with contacts (UB)** The overall goal of this work package is to develop software libraries and software modules to be used as toolbox by the entire project consortium. Since all the deliverables of WP1 were delivered by the end of the third year, the main goal of this WP in the fourth year was to improve the software and enhance the iDyn Library.

**3.2.1.2 WP2: understanding and modelling human whole-body behaviours in physical interaction (JSI)** There were two main objectives within WP2 for the fourth year of the project: (i) to continue the work on unpredictable perturbations of human whole-body behaviour (Task 2.3) and (ii) to continue to study the factors involved in generalization and adaptation of skills learnt in contact with the compliant environment (Task 2.4).

**3.2.1.3 WP3: control and optimization of whole-body motion in contact (UPMC)** The overall objective of this work package is to provide a control architecture dedicated to humanoid robots involved in personal/service applications, which imply physical interactions, i.e. contacts, with the environment. Such a control architecture is a requirement to bridge the existing gap between state-of-the-art methods in humanoid robots control and real-world applications.

During year 4, the objectives of WP3 were mostly focused on Task 3.4. More particularly, partners continued exploring learning approaches for contact situations (unknown location of the contact point, non-rigid contacts) in order to enrich the whole-body control approach de-

veloped in CoDyCo. They also contributed to adaptation methods allowing for the incremental improvement of tasks definitions and their proper activation and prioritization for successful whole-body motions in, potentially unexpected, contact situations.

**3.2.1.4 WP4: adaptation, Generalization and Improvement of Compliant Control and Tasks with Contacts (TUD)** The goal of WP4 is to endow the CoDyCo humanoid robot control architecture with the core abilities for the adaptation, generalization and self-improvement of both control laws and tasks that involve physical interaction with humans, and the environment. In this context, we propose learning approaches that work in conjunction with the control architecture devised in WP3 and rather complement analytical robotic approaches with on-policy learning than starting from scratch. A core idea behind this work package is that Learning should complement classical approaches and not supersede them.

The fourth year objectives of WP4 include:

- Learning how to combine elementary tasks by imitation and reinforcement learning. The combinations involved include the learned simultaneous use of elementary tasks, the sequential use as well as the co-articulation of tasks.

**3.2.1.5 WP5: systems integration, standardization and evaluation on the iCub robot (IIT)** The fourth year main objective for WP5 was the implementation of a validation scenario consisting of the assisted standing up motion.

**3.2.1.6 WP6: management (IIT)** The fourth year management was primarily dedicated to the project concluding activities.

**3.2.1.7 WP7: dissemination and Exploitation (IIT)** The main dissemination objectives for the CoDyCo fourth year were the publication of scientific papers and videos.

### 3.3 Work progress and achievements during the period

#### 3.3.1 Progress overview and contribution to the research field

All the CoDyCo fourth year objectives have been attained. Here is a list of the CoDyCo fourth year achievements.

- 
- 
- 

#### 3.3.2 Work packages progress

**WP1: toolbox for computing and controlling dynamics of whole-body movements with contacts (UB)** WP1 objectives were achieved for the fourth year. In summary, the main accomplishments and impacts for the research community are as follows:

- In T1.3. IIT worked on enhancing the wholeBodyInterface.
- In T1.5. IIT implemented BERDY C++ and sparse matrix representation.
- In T1.3. UPMC kept on improving OCRA.
- In T1.5. INRIA developed different modules for visualization of torques, interfacing a haptic device and learning movement primitives.

**WP2: understanding and modelling human whole-body behaviours in physical interaction (JSI)** In T2.2 and also T2.3, UB continued on improving CoM dynamic manipulability as a tool to study, analyze and measure physical abilities of humans and robots.

In T2.4 UB explored the mechanism of human force perception aiming to provide natural and stable control for a humanoid robot in the similar manner with humans. Through this work, an experimental design has been developed, and a series of human subject experiments examined the anticipated goal-directed behaviour interacting with different compliant force dynamics. They also focused on compliant contacts with support surfaces under uncertainty, where one of the important issues is the extraction of information about the contact surfaces through the sense of touch. UB conducted two psychological studies where they examined tactile roughness through perceptual judgments and brain activation, and one study where they examined the effects of tangential load force uncertainty on precision grip cooperative lifting. Further to these studies, UB developed a preliminary study which was performed using the Haptic master along with a simulated environment.

In T2.4 UPMC analyzed social and physical signals in human-robot (iCub) interaction during a collaborative assembly task. The experiments, performed by Serena Ivaldi at UPMC, were later analyzed during her time in TUD and INRIA.

With a follow-up of the previous work in T2.2, which showed how contacts are established to facilitate goal directed movements, JSI performed a study to answer an inverse question: how would a contact be released? Furthermore (in line with T2.4), if there is an uncertainty of balance, how does this contact preference change?

On their newly developed real-time movable platform perturbation system, JSI investigated effects on balance during quiet standing. A memory task and an inhibitory Stroop task were performed to explore cognitive control over balance in novel challenging conditions.

- 
- 
- 
- 

**WP3: control and optimization of whole-body motion in contact (UPMC)** After the fourth year of project, WP3 objectives were achieved for the fourth year. In summary, the main accomplishments and impacts for the research community are as follows:

T3.3 IIT proposed a control laws ensuring the stabilization of a time-varying desired joint trajectory and joint limit avoidance in the case of fully-actuated manipulators.

T3.3 As part of both WP1 and WP3, UPMC has pursued the generic implementation of an optimisation based whole-body controller named OCRA.

T3.4 TUD and INRIA, in collaboration with WP4, continued the collaboration on the topic of learning torque control in presence of multiple contacts, exploiting the force/torque and tactile sensors of iCub.

T3.4 UB and TUD worked on developing a method to realize desired contact normal forces between a robot's end-effector and its compliant environment.

T3.4 INRIA designed a multi-task prioritized controller with soft task priorities.

T3.4 UPMC developed a task compatibility optimization framework allowing for the incremental adaptation of operational tasks for whole-body control. This framework will be used for the implementation of year 4 demonstration.

T3.4 UPMC pursued the generic implementation of a Model Predictive stepping approach for robust balance.

WP2 JSI and UPMC kept developing a computational model of a reaching controller using the Speed-Accuracy trade-off.

**WP4: adaptation, generalization and improvement of compliant control and tasks with contacts (TUD)** After the fourth year of project, WP4 objectives were achieved for the fourth year. In summary, the main accomplishments and impacts for the research community are as follows:

- Based on the probabilistic movement representation of skills we developed a novel approach for learning task prioritizations from human demonstrations. Our approach follows the concept of "soft" priorities, where a task which is lower in the task-hierarchy can controllably interfere with a higher-priority task.
- We investigated how to generate whole-body "safe" motions, by optimizing the profile of task priorities with respect to a given fitness function under several strict constraints. We studied different black-box stochastic search algorithms to optimize the task priorities in a way that guarantees that constraints are never violated.

**WP5: systems integration, standardization and evaluation on the iCub robot (IIT)**  
The fourth year WP5 activities have concentrated on the fourth year validation scenario. A complete description of the scenario can be found in "D5.4 Validation scenario 4: learning how to stand up with the help of a human caregiver.." which discusses the technical implementation of the fourth year validation scenario (see <https://github.com/robotology-playground/codyco-deliverables/tree/master/D5.4/pdf>). With respect to the state of the art the work progress represents an implementation of well established torques controlled whole-body control strategies. The integration of tactile feedback within the whole-body controller is a peculiarity of the implemented CoDyCo validation scenario and therefore represent a step forward with respect to the current state of the art. At the moment of writing the current

deliverable the iCub tactile sensors cover the feet, the torso, the arms and the hands and the implemented validation scenario accounts for contacts at the hands and feet.

**WP6: management (IIT)** The CoDyCo project management was concluded successfully. Management activities included the definition of an amendment procedure smoothly organized by the consortium and the project officer. The software repository (<https://github.com/robotology/codyco>) was consolidated on github (<https://github.com>).

**WP7: dissemination and exploitation (IIT)** Within WP7, CoDyCo fourth year achievement include: dissemination at relevant academic and industrial events; realization of a CoDyCo experiment database to disseminate robot and humans datasets.

### 3.3.2.1 Work package 1 progress

**Software architecture design and evaluation of available open-source software pertinent to the scope of the project. (T1.1)** The goal of T1.1 was to agree on a specific software architecture with associated software tools whose specifications, dependencies and interconnections meet the requirements and needs for achieving the goals of the project. The software, which is called codyco-superbuild, has been available via github on <https://github.com/robotology/codyco-superbuild> since the second year of the project. Details about the modules of the software are available in deliverables D1.1, D1.2 and D1.3.

**Simulator for whole-body motion with contacts (T1.2)** The CoDyCo project requires a modular, component-based dynamics simulation software providing numerically stable, computationally efficient and physically consistent simulations of whole-body virtual human(oid) systems in contact with rigid or soft environments. During year four the iCub simulator was further developed, keeping it aligned with the robot development.

**Control library for flexible specification of task space dynamics of floating base manipulators. (T1.3)** UPMC has kept developing OCRA over the 4th year of CoDyCo. OCRA stands for Optimization-based Control for Robotics Applications. OCRA is a set of tools which facilitates the development of optimization-based controllers for robots. At its core there is ocra-recipes, a group of platform independent libraries which can be used to quickly develop optimization based controllers for any robot. Hierarchical, weighted, and hybrid controller schemes can easily be implemented using the ocra-recipes libraries. The generic interfaces provided by OCRA allow different robots to use the exact same controllers. Examples of such implementations can be found for the humanoid robot iCub (ocra-wbi-plugins), and the 7 DoF Kuka LWR (ocra-kdl). OCRA also allows users to specify high-level objectives via tasks. These tasks provide an intuitive way of generating complex behaviours and can be specified in XML format. In addition, a variety of gazebo plugins and controller visualization tools have been developed to facilitate debugging and tuning of the controller.

Among these plugins, a predictive approach [1] to preview the duration and placement of coplanar contacts has been implemented in the form of a client for OCRA using the iCub

humanoid robot. Within a model-predictive control framework, the problem is formulated as a linearly constrained mixed-integer quadratic program (MIQP) which allows the determination over a preview horizon, of the optimal changes in the base of support of the robot with compatible CoM behaviour, subject to multiple constraints, while maximising balance and performance of a walking activity.

**Resources:**

- Ocra Home Page and Docs:
  - <https://ocra-recipes.github.io/web/>
  - <https://ocra-recipes.github.io/web/doxy-ocra-wbi-plugins/html/classWalkingClient.html>
- Code:
  - <https://github.com/ocra-recipes/ocra-recipes> – Optimization-based Control for Robotics Applications.
  - <https://github.com/ocra-recipes/ocra-wbi-plugins> – Controller implementations and plugins for communicating between the whole body controller libraries developed at ISIR, ocra-recipes, and the iCub Whole Body Interface, WBI, libraries.
  - <https://github.com/ocra-recipes/ocra-gazebo-plugins> – OCRA related Gazebo plugins.
  - <https://github.com/ocra-recipes/ocra-gui> – GUIs.
  - <https://github.com/kuka-isir/ocra-kdl> – Ocra ROS/RTT/KDL integration.
  - <https://github.com/ocra-recipes/ocra-wbi-plugins/tree/master/ocra-iicub-clients/walking-client> – Walking client for the MIQP predictive control approach.
- Videos:
  - <https://youtu.be/nvoFkYU351U?list=PLsQDs1seNf5uJA-3fUTzILFZ9t7rFlfmP>

During the fourth year, IIT completely refactored the Matlab Simulink Toolbox for whole-body control (WB-Toolbox). WB-Toolbox is a Simulink wrapper to the wholebodyinterface, a C++ library for abstracting the design and synthesis of whole-body controllers without making any preliminary assumptions on the control laws to be implemented. The main advantage of the whole-body interface library with respect to existing control libraries is the decoupling of the control software from implementation details, which are related to the robotic platform. Furthermore, the resulting code is more clean and concise than ad-hoc code, as it focuses only on the implementation of the control law. In this context, the WB-Toolbox Simulink libraries provides support to Model-Driven based development. During the last year, particular effort has been put in improving the robustness, scalability and extendability of the library. Furthermore the library has been rewritten so as to simplify the support to different simulation engines other than Simulink.

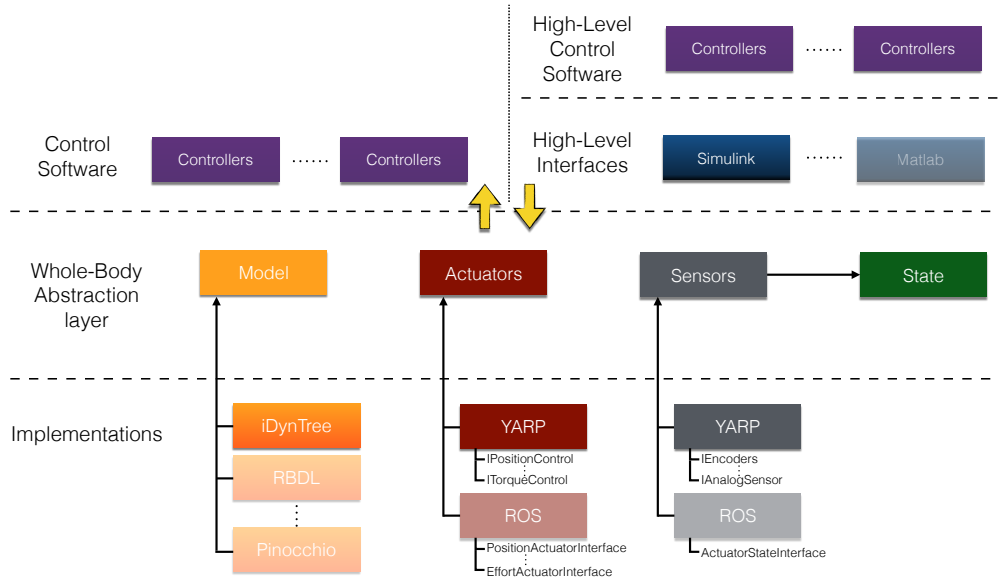


Figure 1: Whole-body Interface software architecture

**System dynamics estimation software. Extension to environmental compliance estimation (T1.4)** The goal of T1.4 was to include compliant contact estimation to the software. This is part of codyco-superbuild software which its details are reported in deliverables D1.1, D1.2 and D1.3.

**Extension and enhancement of the iDyn library. (T1.5)** As part of this task, INRIA developed several software modules which are all available on github. These modules which have been used as a support for the research in the other WPs are:

- software and GUI for visualizing the whole-body torques of iCub: <https://github.com/inria-larsen/icub-wholebody-visualization>
- software for interfacing the Geomagic software with Gazebo and use it for haptic interaction with iCub: [https://github.com/inria-larsen/geomagic\\_touch](https://github.com/inria-larsen/geomagic_touch)
- software for learning prioritized controllers, in Matlab, with implementation of constrained stochastic optimization algorithms: <https://github.com/serena-ivaldi/learnOptimWBC>
- software for learning Probabilistic Movements Primitives from trajectories acquired by demonstrations on iCub: <https://github.com/inria-larsen/icubLearningTrajectories>

During the fourth year, IIT extended the iDynTree library, i.e. the new version of the iDyn library, to support a new probabilistic based estimation algorithm with redundant measurements, called Bayesian Estimation for Robot Dynamics, (BERDY). BERDY algorithm can be used to estimate the dynamics of any mechanical system by adopting a sensor fusion approach.

Indeed, information coming from multiple sensors such as IMUs, force/torque sensors, etc, can be integrated together with their corresponding variance so as to obtain the probability density function of the estimate of the whole-body dynamics of the considered system. When the Gaussian hypothesis is used, the dynamics estimation can be obtained by solving a linear system of equations, which are intrinsically sparse. This led to the implementation in iDynTree of a compressed row storage (CRS) scheme for sparse matrices. Preliminary results seems to report an increment in the computational performance of about 40%with respect to the dense implementation. To ease the development of algorithms and batch data processing, the iDynTree library has been extended to provide support to Matlab scripting. It is now possible to call iDynTree functions directly from Matlab scripts.

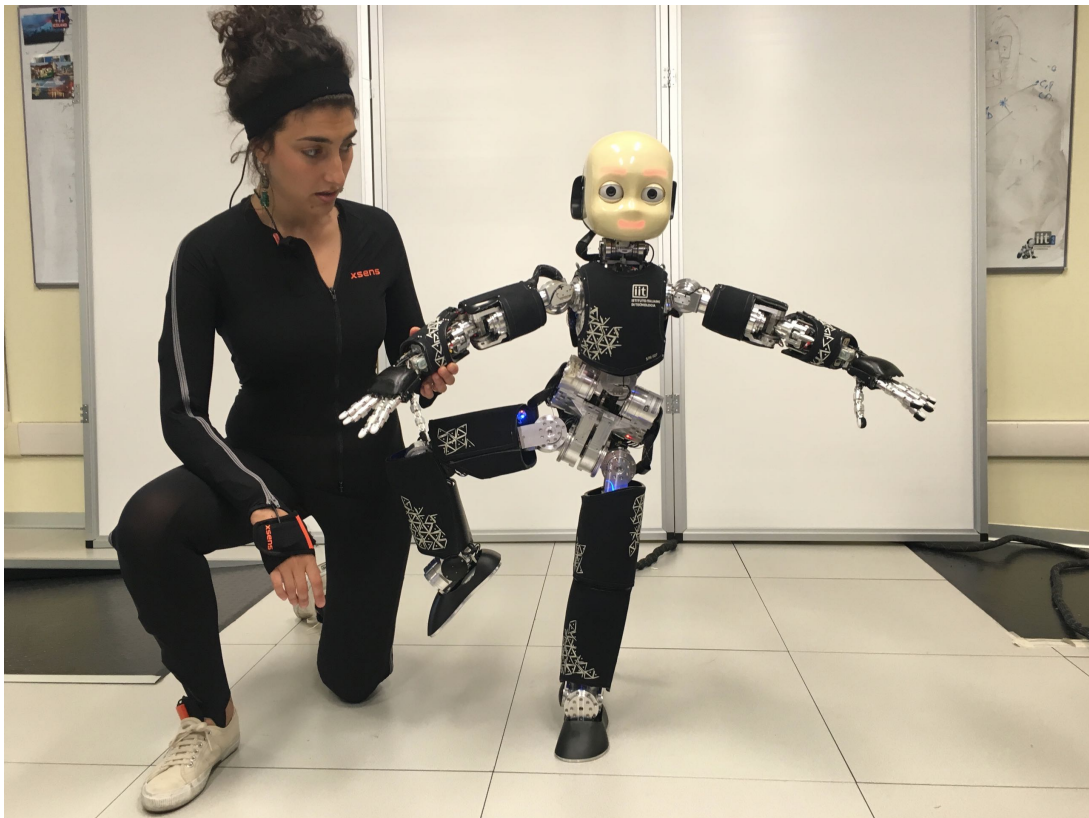


Figure 2: Human interacting with the iCub Robot. The BERDY algorithm can be used to estimate online both the dynamics of the robot and of a human.

**Resources** Overall, the use of resources within WP1 was in accordance to the plans.

WP1 person months	IIT	TUD	UPMC	UB	JSI	INRIA
Year 1	8.67	1.00	3.29	0.51	2.00	-
Year 2	3.00	3.00	0.47	2.29	-	-
Year 3	-	1.00	-	2.18	2.00	2.96
Year 4	?	1.00	1.44	?	2.00	2.06
Partial	?	?	?	?	?	?
Overall	12.00	9.00	6.00	15.00	6.00	5.00

**Deviations from workplan** Overall the project is aligned with the plan.

### 3.3.2.2 Work package 2 progress

**CoM dynamic manipulability as a tool to study, analyze and measure physical abilities of humans and robots** First, the equation for the CoM manipulability ellipsoid was modified to decompose the effect of velocity and gravity related accelerations from the configuration dependent parts. Then, two different choices for the weighting matrix were introduced in order to evaluate the physical ability to accelerate the CoM with certain limits at the joint torques or joint accelerations. Assuming unit weighted norm of actuated joint torques as

$$\boldsymbol{\tau}^T \mathbf{W}_\tau \boldsymbol{\tau} = 1, \quad (1)$$

the modified inequality of the CoM manipulability ellipsoid is

$$0 \leq (\ddot{\mathbf{c}} - \ddot{\mathbf{c}}_{vg})^T (\mathbf{J}_\tau \mathbf{W}_\tau^{-1} \mathbf{J}_\tau^T)^{-1} (\ddot{\mathbf{c}} - \ddot{\mathbf{c}}_{vg}) \leq 1, \quad (2)$$

where  $\mathbf{W}_\tau$  is the weighting matrix and  $\ddot{\mathbf{c}}$  is the CoM acceleration as

$$\ddot{\mathbf{c}} = \mathbf{J}_\tau \boldsymbol{\tau} + \ddot{\mathbf{c}}_{vg}, \quad (3)$$

$\mathbf{J}_\tau$  is a Jacobian that maps joint torques to the CoM acceleration and  $\ddot{\mathbf{c}}_{vg}$  is the velocity and gravity dependent part of the CoM acceleration. The center of this ellipsoid is  $\ddot{\mathbf{c}}_{vg}$  and its radii and orientation can be determined by the eigenvectors and eigenvalues of matrix  $(\mathbf{J}_\tau \mathbf{W}_\tau^{-1} \mathbf{J}_\tau^T)$ . Therefore, the size and shape of ellipsoid is configuration dependent only. Velocity and gravity only alter the location of the ellipsoid within the space of the CoM acceleration.

Different choices can be used for  $\mathbf{W}_\tau$  based on the application. Here, we discuss two reasonable choices that can be used for general purposes.

#### First Choice: Torque Limits

Our first proposed reasonable choice for  $\mathbf{W}_\tau$  is

$$\mathbf{W}_\tau^{-1} = \text{diag}([k\boldsymbol{\tau}_{1_{max}}^2, k\boldsymbol{\tau}_{2_{max}}^2, \dots, k\boldsymbol{\tau}_{k_{max}}^2]), \quad (4)$$

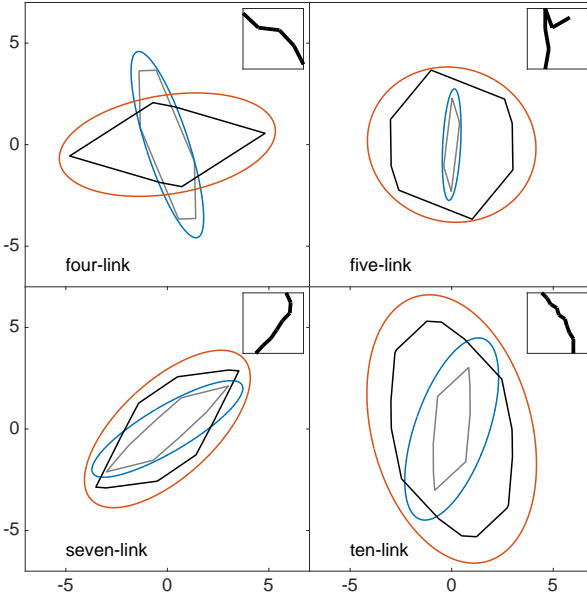


Figure 3: Feasible CoM acceleration polygons due to torque limits and CoM dynamic manipulability ellipses for four different planar robots. The black polygons and red ellipses are for constrained end-effectors whereas the grey polygons and blue ellipses are for unconstrained robots at the same configuration. The gravity and velocity are assumed to be zero ( $\ddot{c}_{vg} = 0$ ).

where  $\tau_{i\max}$  is the saturation limit at the  $i^{th}$  joint ( $i = 1, 2, \dots, k$ ) and  $|\tau_i| \leq \tau_{i\max}$ . By using this weighting matrix, (1) will become

$$\frac{\tau_1^2}{\tau_{1\max}^2} + \frac{\tau_2^2}{\tau_{2\max}^2} + \dots + \frac{\tau_k^2}{\tau_{k\max}^2} = k. \quad (5)$$

Since the ellipsoid in (5) accommodates all combinations of available joint torques (i.e.  $\tau_i^2/\tau_{i\max}^2 \leq 1$ ), the outcome ellipsoid in (2) will include all achievable accelerations of the CoM.

In order to verify our choice of  $\mathbf{W}_\tau$  and to illustrate the relationship between manipulability ellipsoid (ellipse in 2D) by using (4) and achievable CoM accelerations due to torque limits, we plot ellipses for four different planar robots at zero velocity and gravity (i.e.  $\ddot{c}_{vg} = 0$ ), assuming arbitrary torque limits. These four robots consist of (i) four, (ii) five, (iii) seven and (iv) ten links which are connected to each other by active revolute joints. The first link of each robot is fixed to the ground by a passive revolute joint. Each link is assumed to have unit mass and length and its CoM in the middle. Corresponding robots configurations, which are chosen randomly, are depicted in the top right corner of each plot. Areas of feasible CoM accelerations (due to saturation limits) for these robots are indicated in Fig. 3 by grey and black polygons. These polygons are obtained numerically by mapping points inside the range of available joint torques ( $|\tau_i| \leq \tau_{i\max}$ ) to the CoM acceleration space. This mapping is done by using (3). Both polygons for each robot are for a same configuration. The difference is that the black one shows the achievable area when the end point of the last link is fixed (i.e. an extra bilateral constraint). This is to show the effect of an additional constraint on feasible CoM accelerations (and also on ellipses). The extra constraint deforms the feasible

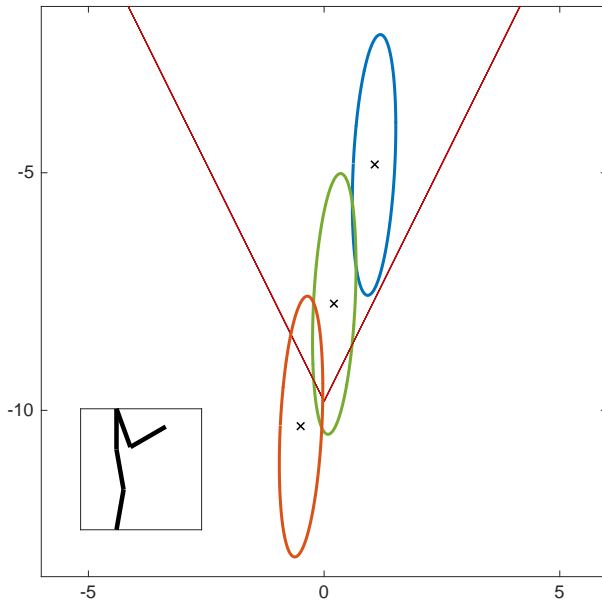


Figure 4: CoM dynamic manipulability ellipses for a five-link planar robot in different velocities. The robot's configuration is shown on the bottom left corner. Straight lines show the friction cone of the contact force.

area due to (i) the additional kinematic constraint limiting the movements of the CoM in some directions, and (ii) contact forces provide additional torques in some directions. Corresponding manipulability ellipses, which are calculated by using the weighting matrix in (4), are also shown in Fig. 3. Red and blue ellipses are related to constrained and unconstrained last links, respectively. Comparing the ellipses and polygons, it can be seen that, by employing (4) as a weighting matrix, these ellipses can provide reasonable approximations of achievable CoM accelerations. It is obvious that calculating ellipses is computationally much more efficient rather than obtaining polygons. Ellipses also provide analytical metrics which can be used to study and optimize a robot's physical ability to manipulate its CoM.

Including gravity and velocity to the above examples will only change center points of the polygons and ellipses and will have no effect on shapes and sizes of those areas. As an example, we consider the five-link robot in the same configuration and same torque limits as we had for the ellipses in the top right corner of Fig. 3. The robot's configuration is shown in the bottom left corner of Fig. 4. The blue ellipse in this figure is the CoM manipulability ellipse for this robot when the gravity exists and velocity is zero. Therefore, the difference between this ellipse and the blue one in the top right corner of Fig. 3 is due to the gravity which only moves the center point ( $\ddot{c}_{vg} \neq 0$ ). The red and green ellipses in Fig. 4 are also for the same robot and same configuration but different velocities. This implies a kind of decoupling between the effects of inertial parameters and configuration (size and shape of the ellipse) on one hand and velocity (location of the ellipse) on the other hand. This decoupling is important in studying physical ability of a robot in different configurations independent of its velocity.

The inequality (2) for the CoM dynamic manipulability ellipsoid is derived assuming that the contacts are bilateral. Although in legged robots the contacts are usually unilateral, it is desired to maintain the contacts (except contact switching) and prevent sliding or loss of

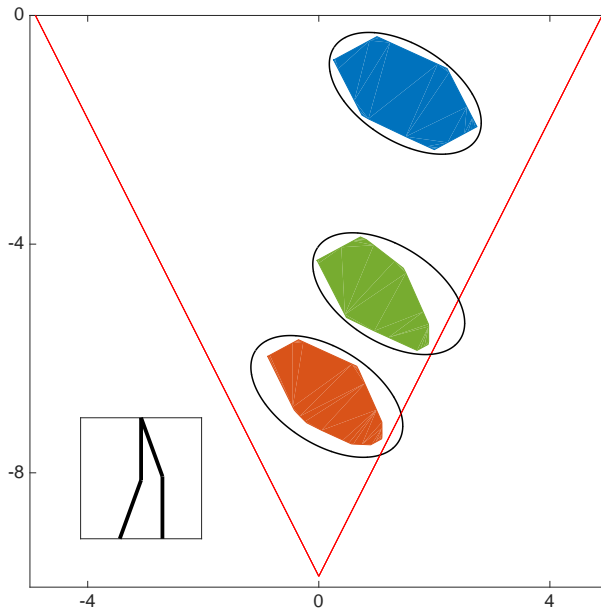


Figure 5: CoM dynamic manipulability ellipses and feasible CoM acceleration polygons due to torque limits and unilateral constraints of a four-link robot with two contact points in different velocities. Straight lines show the friction cone of the total force.

contact during the robot's performance. Therefore, bilateral contact assumption still makes sense if the contact forces satisfy the unilateral contact constraints. In the example in Fig. 4, replacing the bilateral constraint by a unilateral one in the first link, we can draw friction cone constraints in the CoM acceleration space. Straight lines in Fig. 4 show the CoM acceleration limits due to the friction cone when the coefficient of friction is 0.5. As can be seen in this figure, different velocities result in different feasible areas for a same manipulability ellipse due to the unilateral constraint. It implies that, although the CoM dynamic manipulability ellipse, which is an approximation of the robot's physical ability to accelerate its CoM, remains the same, enabling the robot to exploit that ability is dependent on velocity, as well. Note that, a proper velocity has to be determined by a controller (or a motion planner) in order to exploit available ability of a robot to reach a certain acceleration of the CoM and satisfy the contact conditions.

In the examples in Fig. 4, we assumed a unilateral constraint at the first link of the robot which is the same situation that arises in single support phase for legged robots. Since we also assumed that the first joint is unactuated, the CoP (and also the ZMP) is always at the contact point no matter if the robot is in balance or not. This clarifies the difference between the CoP (or the ZMP) and manipulability ellipses. As can be seen in Fig. 4, ellipses provide information about the robot's ability to accelerate the CoM in different directions with different configurations and velocities, whereas the CoP (or the ZMP) remains at the same point regardless of the robot's states.

It is worth mentioning that a larger ellipse means not only higher physical ability to accelerate the CoM, but also larger feasible region for  $\ddot{c}_{vg}$  to include a desired point in the CoM acceleration space inside the ellipse. In other words, although the ellipse's position and therefore its feasible part due to the unilateral constraint is dependent on  $\ddot{c}_{vg}$ , having a larger

ellipse provides more options for the controller (or the planner) to choose a proper velocity to reach a desired CoM acceleration.

Introducing more unilateral constraints to the robot (e.g. double support phase in legged robots), or having multiple contacts which at least one of them is unilateral, will result in velocity dependent limits for the CoM acceleration. In this case, each contact has its own friction cone limits which are dependent on robot's states. This is due to the relationship between contact forces and robot's velocity. Fig. 5 shows manipulability ellipses and their corresponding feasible CoM acceleration areas of a four-link robot in three different velocities. The polygons are obtained numerically and by using (3). The robot's configuration is depicted in the bottom left corner of the graph and it is chosen to mimic double support phase of a planar biped. The blue (top) area shows the feasible area when the velocity is zero and the two others are for randomly chosen velocities. By comparing the three areas, it is obvious that different limits are affecting feasible areas at different velocities which shows the dependency of the limits on the robot's velocity.

As can be seen in Fig. 5, manipulability ellipses are the same for all velocities implying that the robot's physical ability to accelerate its CoM does not depend on velocity. However, the robot's velocity affects the feasibility of the areas due to the unilateral contacts. In other words, in all three velocities, the robot's physical ability to accelerate its CoM is the same, although in two of the velocities (i.e. green and red areas) the robot may lose its contact with the ground if it wants to reach certain accelerations. Therefore, exploiting robot's ability in a certain configuration depends on choosing proper velocity by the controller (or planner), as well. Note that, straight lines in Fig. 5 show the friction cone limits for the total contact force which do not have any effect on feasible areas at the chosen velocities since the areas are already limited by friction cone constraints of individual contact forces.

## Second Choice: Joint Accelerations

Other than joint torques, joint accelerations are also important factors in studying a robot's physical ability. Obviously, producing less accelerations at the joints, with same amount of joint torques and same CoM acceleration, is desirable since it leads to lower joint velocities and consequently less joint movements. Less movements at the joints is beneficial since the robot's workspace is limited. Also lower joint velocities with same joint torques means less work and higher energy efficiency. Therefore, we introduce a proper weighting matrix in order to study the robot's CoM acceleration due to the limited joint accelerations.

Let  $\mathbf{W}_q \in \mathcal{R}^{n \times n}$  denote a symmetric positive definite matrix. We define the second choice of  $\mathbf{W}_\tau$  as

$$\mathbf{W}_\tau = \mathbf{J}_q^T \mathbf{W}_q \mathbf{J}_q. \quad (6)$$

By substituting (6) into (1), we will have

$$\boldsymbol{\tau}^T \mathbf{W}_\tau \boldsymbol{\tau} = 1 = \boldsymbol{\tau}^T \mathbf{J}_q^T \mathbf{W}_q \mathbf{J}_q \boldsymbol{\tau}. \quad (7)$$

Given that  $\ddot{\mathbf{q}} = \mathbf{J}_q \boldsymbol{\tau} + \ddot{\mathbf{q}}_{vg}$ , the above equation becomes

$$(\ddot{\mathbf{q}} - \ddot{\mathbf{q}}_{vg})^T \mathbf{W}_q (\ddot{\mathbf{q}} - \ddot{\mathbf{q}}_{vg}) = 1, \quad (8)$$

where  $\mathbf{W}_q$  can be used to unify the units or express the relative importance of the joint accelerations in  $\ddot{\mathbf{q}}$ .  $\mathbf{J}_q$  is a Jacobian that maps joint torques to the joint acceleration and  $\ddot{\mathbf{q}}_{vg}$

is a part of the joint accelerations due to gravity and joint velocities. The above equation specifies a n-dimensional ellipsoid in the joint acceleration space which its center point is at  $\ddot{\mathbf{q}}_{vg}$ . This point is the same center point of a n-dimensional ellipsoid that will be obtained if we project the unit weighted norm of joint torques (i.e. Eq. (1)) to the joint acceleration space. Such ellipsoid will be the same as (2) if we replace  $\mathbf{J}_r$  with  $\mathbf{J}_q$  and  $\ddot{\mathbf{c}}$  with  $\ddot{\mathbf{q}}$ .

By choosing  $\mathbf{W}_r$  as in (6), CoM dynamic manipulability ellipsoid will show an area in the CoM acceleration space which is achievable via unit weighted norm of joint accelerations in (8). Therefore, by setting proper values for  $\mathbf{W}_q$  (user's choice based on the application), a user can study the effect of joint accelerations on reaching desired CoM accelerations. As an illustrative example, Fig. 6 shows CoM manipulability ellipses for a five-link planar robot (i.e. the same robot explained earlier in this section) in two different configurations which are shown in bottom left corners of the plots. Without losing generality, we set the gravity and velocity to zero in these examples (i.e.  $\ddot{\mathbf{q}}_{vg} = \ddot{\mathbf{c}}_{vg} = 0$ ). Torque limits for all four actuated joints are assumed to be one. Green areas show feasible CoM accelerations due to the torque limits and green ellipses are their approximations which are obtained by using (4). Blue and red areas indicate CoM accelerations which are achievable by limited norm of the joint accelerations. For the blue areas the norm is one (i.e.  $\ddot{\mathbf{q}}^T \ddot{\mathbf{q}} = 1$ ) and for the red ones the norm is 3 (i.e.  $\ddot{\mathbf{q}}^T \ddot{\mathbf{q}} = 9$ ). Blue and red ellipses are obtained by using (6) and setting  $\mathbf{W}_q$  to identity and 1/9 times identity matrices, respectively, to match the corresponding areas. Green, blue and red areas are obtained numerically and by using (3). In obtaining red and blue areas corresponding joint acceleration limits (i.e.  $\ddot{\mathbf{q}}^T \ddot{\mathbf{q}} \leq 1$  for red areas and  $\ddot{\mathbf{q}}^T \ddot{\mathbf{q}} \leq 9$  for blue areas) are also considered.

As it is expected, and also can be seen in Fig. 6, blue and red ellipses include all points in the blue and red areas, respectively. Although they also include points which are not inside their corresponding areas. The reason is that the mapping from the joint acceleration space to the CoM acceleration space is not one-to-one, which means that the mapping from the CoM to the joint acceleration space may be different. Comparing the two examples in Fig. 6, it is obvious that in the top configuration, although the green area is smaller, the blue and red areas are larger compared to the bottom plot. It means that, the same CoM accelerations can be achieved by generating smaller accelerations at the joints in the top configuration comparing with the bottom one. This can be explained by CoM dynamic manipulability ellipses as the blue and red ellipses are much more aligned with the green one in the top plot rather than in the bottom one. Note that, blue and red ellipses have the exact same alignments and the only difference is in their sizes. Therefore, in order to minimize the norm of the joint accelerations to reach a certain CoM acceleration, one can minimize the difference in the alignments of these two ellipses.

Since the proposed metric studies the motion of the CoM, which is the main focus in balancing motions of robots, it can be used to evaluate a robot's ability to balance. Thus, we define *physical ability to balance* as a robot's physical ability to manipulate its CoM in the horizontal directions. Therefore, if we project dynamic manipulability ellipsoids of a robot, in different configurations, onto the horizontal plane, the configuration with the largest ellipse (i.e. projected ellipsoid) will have the highest ability to balance in the sense of the required torque if we use (4) or the required joint accelerations if we use (6). Note that, the largest projected ellipse is not necessarily the projection from the largest ellipsoid, since the largest ellipsoid might be extended in another (i.e. the vertical) direction. Therefore, by using the

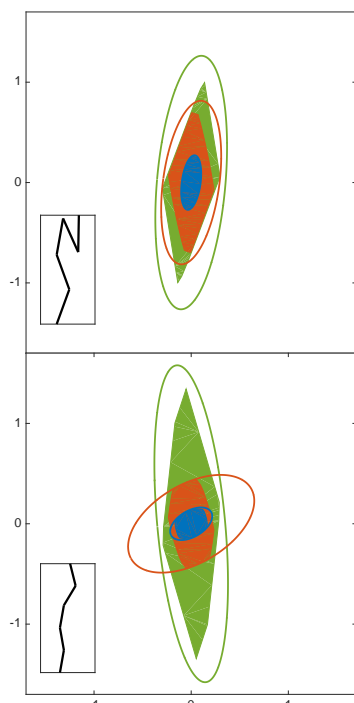


Figure 6: CoM dynamic manipulability ellipses with different weighting matrices for a planar five-link robot in two configurations. Green areas show feasible CoM accelerations due to torque limits. Blue and red areas show achievable CoM accelerations with unit weighted norms of joint accelerations.

CoM dynamic manipulability one can compare different configurations of a robot] or even different robots in terms of their physical abilities to maintain balance.

**Human learning compliant force dynamics through physical interactions** To explore the mechanism of human force perception has a key role in the CoDyCo project, aiming to provide natural and stable control for a humanoid robot in the similar manner with humans. Through this work, an experimental design has been developed, and a series of human subject experiments examined the anticipated goal-directed behaviour interacting with different compliant force dynamics. Three different types of forces (a simple linear and two non-linear forces) were generated by a haptic device, and the human movements were measured against the compliant forces. The participants were asked to set the half-position and half-force after the certain repetitive movements to reach the target. The results showed that although humans were more sensitive to the position control than the force, they could differentiate the three dynamics. Interestingly humans seem to be more sensitive to the total power to the target than the point-force at the target. Moreover, the learning performance was also analysed and the learning curves were different between the three, suggesting some relations might exist in everyday real activities. As such, the work has deepened the understanding how humans perceive the force to reach anticipated goals ruled by the certain dynamics. This would be beneficial to apply it for providing not only natural human-robot interaction but also stable humanoid robot control when interacting with multiple compliant surfaces.

The study about human force perception and learning through compliant contact dynamics helps to design and develop a more natural and dynamical contact to humanoid robots. To explore the human learning compliant force dynamics through physical interactions, we generated four different compliant forces (two linear and two non-linear cases) by changing the stiffness values (See Figure 7).

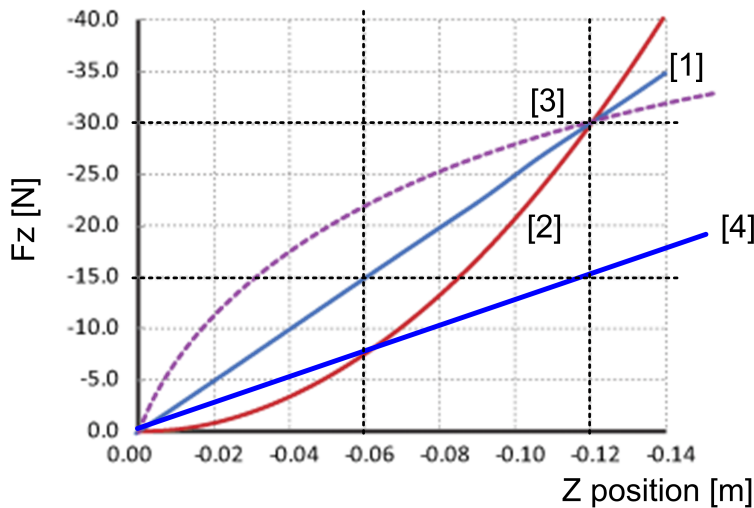


Figure 7: Four different force dynamics are applied. [1] Linear, [2] Non-linear (quadratic), [3] Non-linear (concave), and [4] Half-linear. The [1],[2],[3] are the same force at the end position (e.g., z=-0.12), and [2] and [4] are the same force at the half position (e.g., z=-0.06).

The stiffness values were calibrated depending on the goal position and the maximum force to be applied at this set position. The participants were asked to set the half-position and half-force after a certain repetition in order to be probed their responses whether or not they properly perceived the force dynamics. Figure 8 shows that although the performance tended to overshoot at both test trial due to the deprivation of the visual information of the target, the participants set the half-position in the similar manner regardless of the force dynamics. Conversely, there were significant differences between the three conditions at the half-force test trials.

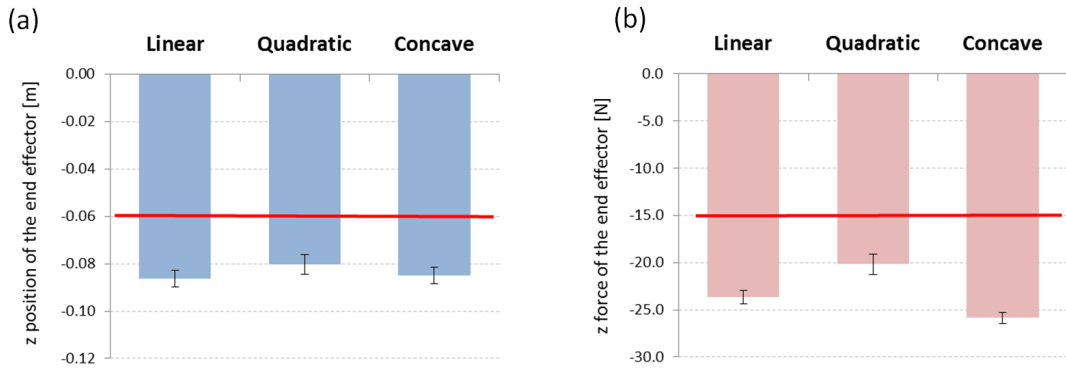


Figure 8: The test trial performances averaged across 18 participants.(a) the end-effector position at the test half-position trial and (b) the applied force at the test half-force trial. The red lines indicate the ideal values based on the dynamics (see Figure 1).

The dynamic learning evaluation revealed that there were significant differences between three forces in the learning performance averaged across 18 participants (see Figure 9). The concave force was not natural, and it was needed several repetitions to understand the dynamics and also to learn how to maintain the accuracy in reaching a target. In contrast, the linear force had less efforts but the learning model maintained a stable conditions after the repetitions. The quadratic force seemed to be a well known or natural force among the three, but still the performance gradually improved over the course of trials. These results suggest that the force model helps the user to achieve more precise and accurate movements.

**Tactile attention and memory in multi-finger contact** Given CoDyCos focus on compliant contact with support surfaces under uncertainty, an important issue is the extraction of information about the contact surfaces through the sense of touch. Knowledge about surface texture, for example, roughness which affects friction and hence contact dynamics, may be derived from static or sliding contact. Two psychology studies at UOB have examined tactile roughness through perceptual judgments and brain activation, while a third study has examined the effects of tangential load force uncertainty on precision grip cooperative lifting.

People often use several digits simultaneously to touch surfaces. Thus, they may use two fingers (eg index and middle) side by side (e.g. in steadyng themselves against a stable surface) or they might use thumb opposing the index (and possibly other fingers) to form a precision grasp on either side of an object (e.g. stair rail). Often the surfaces contacted by the two digits

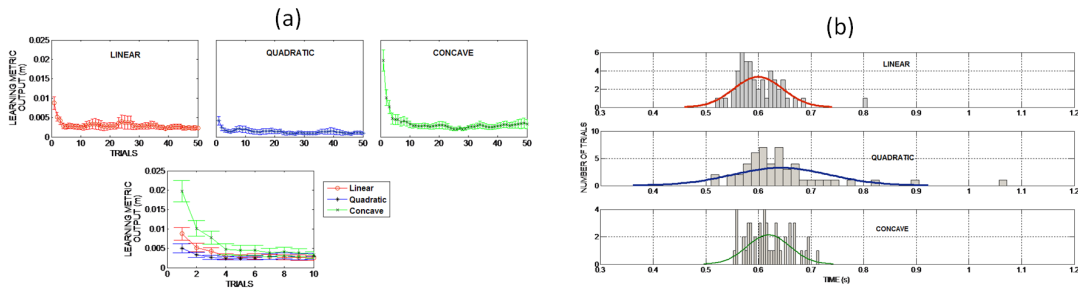


Figure 9: (a) Learning performance of the 18 participants along with the standard error. A big variation in the learning performance of the three different forces is observed within the initial 10 trials. (b) Average time taken by the 18 participants to reach the target with the three different forces.

will be the same and the double contact affords improved tactile sensitivity over single contact. However, two surfaces that are not co-located may differ in texture. For example, when using precision grip to feel fabric, the front and back surfaces may have very different textures. The perceived texture of either surface is then likely to be affected by the surface on the reverse side. We have been investigating such contact in terms of interactive effects on roughness judgments arising from simultaneous contact with two separate surfaces. Depending on the two digits involved, we have shown attention and neural cross talk afford explanations of some of the effects seen [2, 3]. Within CoDyCo we have been contrasting two forms of perceptual judgment, based on single (magnitude estimation) and two successive presentations (2-interval forced choice) of the surfaces. The theoretical interest is in the potential role of short term tactile memory in the second case. Similarity of the two digit judgments despite differences in working memory requirements in the different perceptual tasks inclines us against a significant role for a memory component in multi-digit roughness perception. A paper is in preparation on this topic.

**Surface roughness effects on brain activation in static and sliding contact** Duplex theory proposes that surface roughness judgments are mediated by a combination of vibratory and spatial inputs from the slowly and rapidly adapting tactile mechanoreceptors [4]. Tactile processing by the brain primarily involves the somatosensory cortex. However, cortical areas primarily associated with auditory and visual input can also be involved. Thus, recently it has been shown that direct current stimulation of the visual or auditory cortex can facilitate spatial or temporal tactile judgments [5]. We are currently completing a brain imaging study in which we expect to demonstrate a neural basis for duplex theory. Thus we expect moving sliding textures will activate auditory cortex while static coarse textures invoke visual cortex; preliminary data in Figure 2 show auditory cortex activation with sliding contact.

**The role of uncertainty in shared control of grip in cooperative lifting** Social processes in cooperative multi-person action is a major topic in psychology, but there has been very little analysis of kinematics and dynamics of joint action. We have been examining control of precision grip force during a 2-person lifting task in which the load to be lifted varies from trial to trial. There are three conditions that manipulate load uncertainty. In the first condition the weight is unknown to either participant. In the second condition it is known to just one of the participants, while in the third condition it is known to both of them. We find

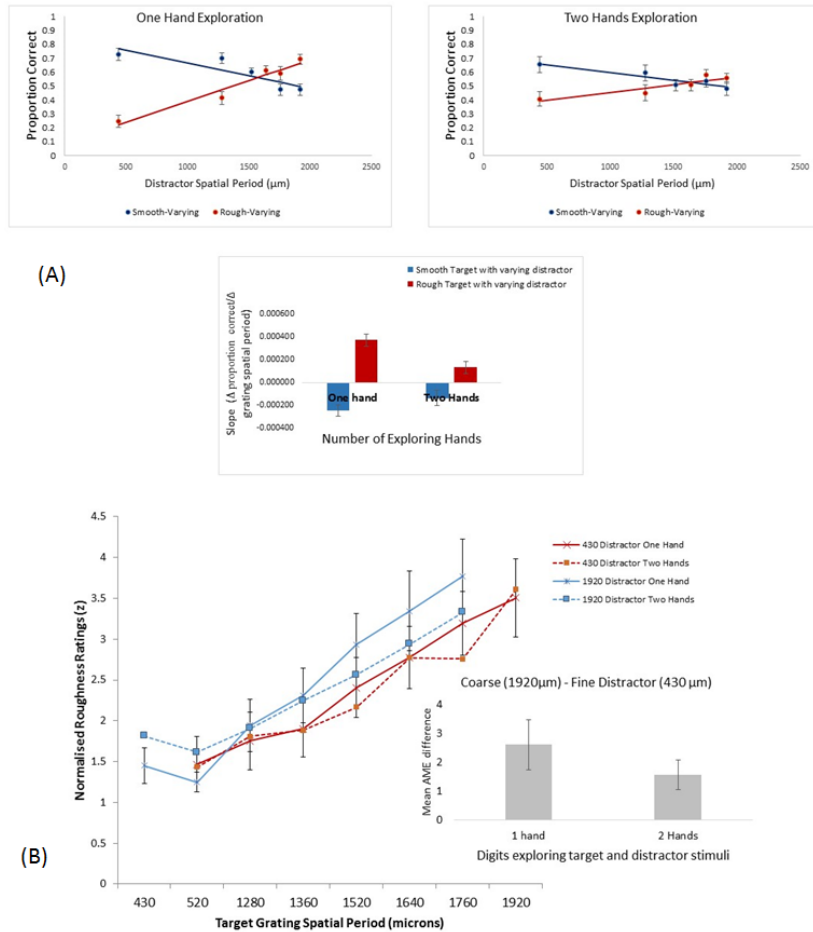


Figure 10: Multifinger contact effects on (A, above) 2-interval force choice (2-IFC) and (B, below) absolute magnitude estimates (AME) measures of roughness perception. In both tasks participants actively explored a target and distractor surface simultaneously using 2 digits; the digits were either on one hand or two hands, expected to result in more or less crosstalk. In the 2-IFC task (A), participants identified the rougher of a pair of target stimuli and were instructed to ignore the distracter. The red circles and line indicate group ( $N=12$ ) average performance when the fine surfaced target was paired with various coarse distractor surfaces; a fine distracter depresses accuracy more than a coarse distracter. The blue circles and line show behaviour with the coarse target; a coarse distracter depresses accuracy more than does a fine one. The bar graph summarising mean slope across participants shows the distraction effect is greater in the one hand condition. In the AME task (B), participants rated the roughness of target surfaces while instructed to ignore the simultaneously touched distracter. The graph at the top of figure 1b shows mean ratings for each target surface. The blue crosses and squares show mean ratings for each target surface with a coarse distracter surface. Mean ratings with a fine distracter surface are shown in red. It can be seen that a coarse distracter results in higher roughness ratings than does a fine distracter. As with 2-IFC, the distracter effects are greater with the distracter on the same hand as the target.

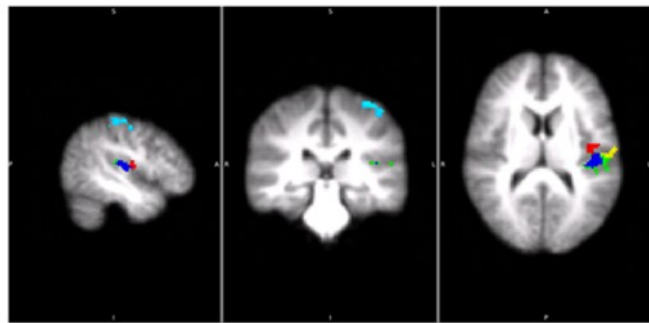


Figure 11: Activations during passive touch. The three panels indicate sagittal, coronal and horizontal planar sections of the brain with multisensory activations for a tactile discrimination task contrasting coarse and fine texture perception under moving and static touch conditions. Regions of interest shown with coloured blobs, were more activated for moving (vs static) touch, including auditory cortex (TE1.0). The stimuli were applied to the right index finger of passive participants, N=13; Light blue: BA1, Green: OP1, Red: OP3, Yellow: OP4, Blue: TE1.0

systematic changes in anticipatory grip as a function of both ones own knowledge but also what is known by ones partner (see Figure 12).

**Human arm impedance characteristics in a dynamical contact task** Studies on human behaviour models with specific relation the arm movement while performing dynamical tasks have been used to understand the principles behind human arm impedance[6, 7]. The effect of such impedance can be a result of the active forces (resisting or assisting) applied by the muscular reflexes, contractions and any specific joint limitations of the movement. From the literature, it is understood that the directional influence of such movements has a direct influence in the arm stiffness or impedance specifically being anisotropic under static conditions [8]. These arm impedance characteristics have also been studied using a virtual model, while the human arm is trying to influence the virtual system by performing a dynamic task [9]. Tee et al.,[10] developed a computational model to study the effect of human arm impedance and the joint stiffness measures observed while trying to perform a task in any given dynamic environment (stable or unstable). These studies focus mainly on the human arm impedance models in a static or dynamic task which will help understanding the human impedance performance in any environment.

As part of the CoDyCo project, the human behaviour model while in contact with compliant forces were analysed and studied previously. Further to this analysis, it is interesting to understand the similar behaviour while in contact with a robot model or any defined object with significant dynamic influence. These intentions led to the development of the following preliminary study which is performed using the Haptic master along with a simulated environment. The goal of this task is to understand how humans emulate or modify their course of action and perception in maintaining the postural balance of a robot model.

## Methods

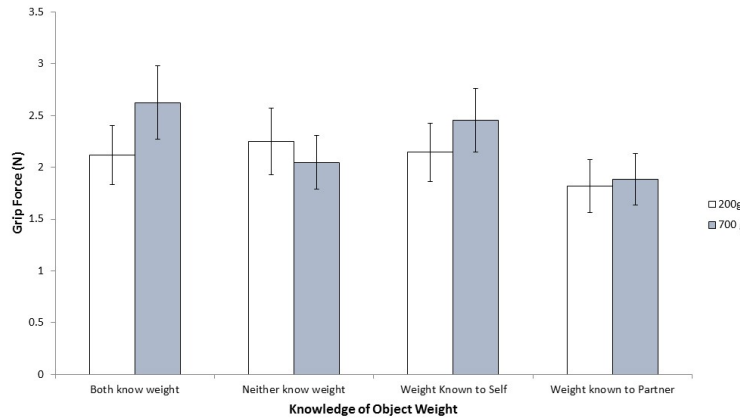


Figure 12: Joint lifting action. The participants worked in pairs to lift a bar to a target height. The weight at the centre of the bar (either 200g or 700g) was known to one, both or neither participant in pair. The force with which the participants held the bar in anticipation of a lift in the different knowledge conditions is shown along with on SE of the mean.

The human arm impedance behaviour can be studied by constraining or limiting the human movement within a specific range. Further, a dynamic task is also needed which will encourage the human to engage in continuous movement. This continuous exploration and the variation in the human arm behaviour will help in understanding the principles behind the mechanical stiffness of the human arm. Further, to answer the global objective of the CoDyCo project, we designed the dynamical task as to help or assist the humanoid robot from a sitting position to the standing position.

The robot model is designed as simple planar double inverted pendulum model which will vary its performance with respect to the velocity and the force parameters received from the Haptic master. The dynamic equation for an inverted pendulum model can be represented as

$$\ddot{x} = g/m + F_{ext}/m + F_{con}/m \quad (9)$$

$F_{ext}$  is the external force received from the Haptic Master input and  $F_{con}$  is the controller force (PD controller) in the knee joint (to maintain the constrained movement). The force applied by the human via the Haptic Master device, is transformed directly to the end-effector position of the planar robot model. The force applied at the end effector is then transformed to the individual joint torques using the following computation:

$$\tau = J^T * F_{ext} \quad (10)$$

with  $\tau$  being the joint torque to be applied in the hip, knee and ankle joints of the robot model.  $F_{ext}$  corresponds to the force applied by the human and measured through the Haptic master device.

To maintain the initial sitting position of the joints the model needs to be equipped with a PID controller or a COM based balancing controller which will further act depending on the force applied by the human through the Haptic Master.

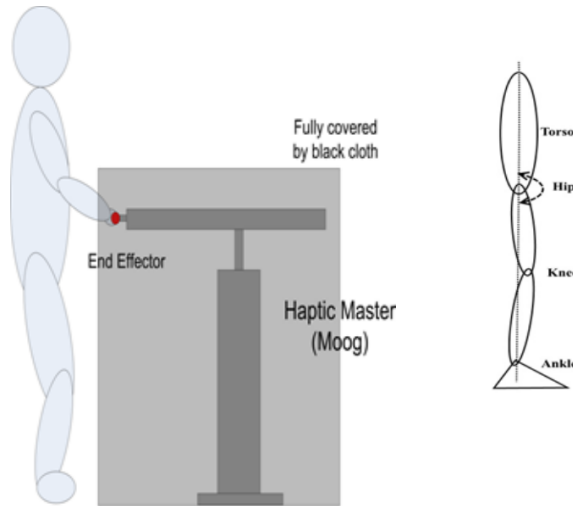


Figure 13: The spring model in the Haptic API is used to emulate the performance of a robot model (mass) and the human applies the force along the x and z directions similar to a planar movement which is visualized using the model in real time.

### Experimentation

The experimental setup involves the Haptic Master device which helps in emulating the human applying the necessary force to initiate the robot (model) to move from a sitting position to standing position. A planar robot model is developed using Simulink and it is directly integrated with the x and z direction forces applied by the participants. The haptic master is also limited to the planar movement which helps the human in controlling the applied moment or contact force. A real time visualization of the planar model is displayed in the monitor which helps the participant to understand and to control the arm movements.

Figure 13 presents the experimental set-up used in this analysis, the Haptic Master moog and Simulation model. Participants will visualize the pendulum model as a visual feedback and can relate the change in the movement depending on the force applied. The static (iso-metric) force model is with high stiffness emulating the body weight and the force feedback from the human is taken as a direct input.

### Preliminary Results

A preliminary study was conducted to evaluate the objective of combining the dynamical task along with restricted human arm movement. This analysis help to understand the behaviour of the low level controller used in the model and influence of the human applied forces. Figure 14 illustrates the external force observed as a result of the applied forces along the x and z axis. The participant was performing a planar motion by applying force along the x and z axis within a given free space. The forces observed to be varying continuously which signifies the dynamically exploration of the user whilst maintaining a higher forces. The real time visualization of the model helped the user to increase or decrease the forces along x and z directions such as to control the movement of the planar robot model.

The observed torque behaviour in all the three joints of the planar model are presented in fig 15. The initial joint torques are applied based on the input from the controller which later on combines with the output from the haptic master. The torque performance explains the movement followed in the planar model, with respect to the user applied forces. The torques

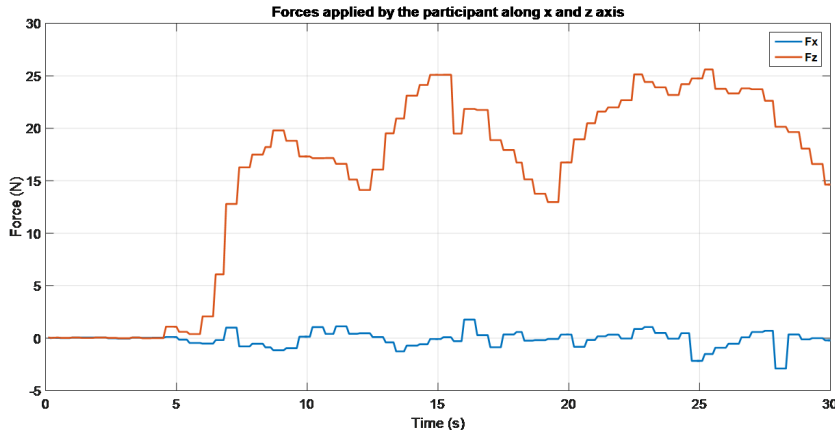


Figure 14: External forces applied by the participant along the x and z axis are measured using the Haptic Master device.

profile stabilises at the end of 30seconds time window which is also in relation to the stabilised forces observed in fig. 14.

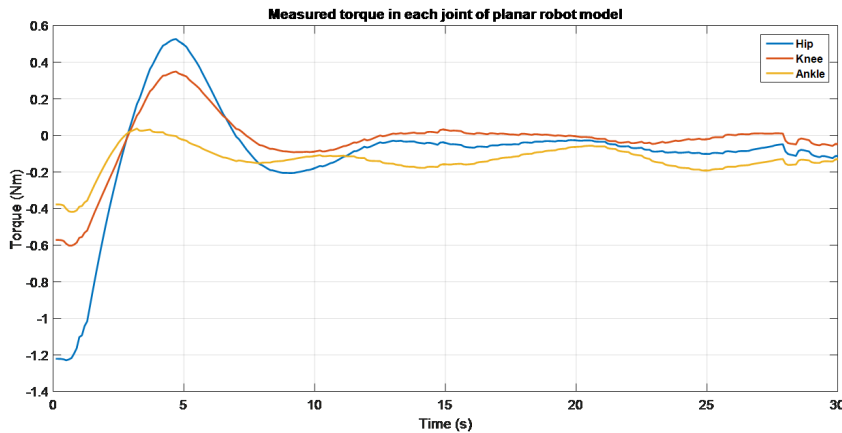


Figure 15: Resulting torque applied to the planar robot model, The torque performance varied depending on the External force applied by the user and the controller output.

**Analysis of social and physical signals in human-robot interaction during assembly task** We analyzed the social and physical signals exchanged by 56 human participants and the iCub during a collaborative assembly task. The experiments, performed by Serena Ivaldi at UPMC, were later analyzed during her time in TUD and INRIA. First, we focused on social signals. In Ivaldi et al. [11], we reported the analysis of results concerning the influence of individual factors in gaze and speech. We found that the more an individual is extrovert, the more he/she will tend to talk to the robot; the more an individual has a negative attitude towards robot, the less he/she will gaze at the robots face and the more he/she will tend to look at the robots hands, where the physical interaction occurs. In Anzalone et al. [12] we also showed that it is possible to predict the extroversion of an individual from a thin slice of face to face interaction between the human and the robot, by taking into account

several movement metrics. We later started to analyze the physical signals, in particular the forces at the end-effectors of the robot (hands) where people were grasping the robot to drive and show the movement. We observed many interesting facts: the variance of median contact forces is smaller in men than women; older people apply smaller forces; extroverts also apply small forces; by contrast, people with negative attitude towards interactions with robots (a subscale of NARS) apply bigger forces. We observed a visible difference between the demonstrations by the expert and the demonstrations provided by the participants, that were not robotics experts: the difference is highly visible, especially in terms of the variability of trajectories and different strategies adopted by the participants when moving the robot arms. Nevertheless, we observed a learning effect in the trajectories demonstrated by the participants: the smoothness of the movement, measured by the log-dimensionless jerk computed on the trajectories, increases across 3 trials in a significant way. A paper summarizing these results is currently in preparation.

**Stepping in a novel balance environment** High stepping reaction time is a predictor of future falling [13], possibly due to inadequate weight shifts preceding foot lift-off [14][15]. These can occur due to external balance perturbations [16] or incorrect planning [14][15]. Thus, incorrect weight shift planning might be linked to falls [17]. To investigate the effect of incorrectly scaled weight shifts on stepping, we developed a novel robotic platform able to amplify subjects weight shifts in real-time.

### Methods

Eleven young adults ( $23.7 \pm 4.6$  years) stepped as fast and accurate as possible to a target suddenly illuminated in front of one of their legs. On 1/3 of the steps the target jumped shortly before foot liftoff, forcing quick and potentially destabilizing adjustments. This task was performed on a moveable platform in three conditions: platform still (baseline, 60 steps and post-adaptation, 30 steps) or moving (adaptation, 90 steps). When moving, the platform doubled subjects mediolateral center of mass movement (COM) in real time. Thus, subjects had to plan a smaller COM movement to generate a weight shift appropriate for stepping to targets. We calculated stepping errors (distance between the target and the foot at landing), step onset time (time between target onset and foot liftoff) and step execution time (time between liftoff and landing). Overall performance was analyzed using rANOVA (target jump x condition) and differences between the first and last five steps of each condition using paired samples t-tests.

### Results

Target jumps increased step execution times and stepping errors (by 50 ms and 49.5 mm, both  $p < .01$ ). Step onsets were delayed in adaptation (by 7 ms), but faster in post-adaptation (by 24 ms). Target jumps delayed step onset by 10 ms in baseline and adaptation (condition x jump interaction,  $p = .03$ ). Step onsets were faster in the first 5 steps of post- adaptation, compared to last adaptation steps (by 37 ms,  $p = .01$ , jump). Stepping errors increased at the start of adaptation (by 19.5 mm,  $p = .02$ , no jump), but decreased over time, within adaptation (by 21.8 mm,  $p = .03$ , target jump) and post- adaptation (by 7.5 mm,  $p = .047$ , no jump).

### Conclusions

When targets jumped, stepping errors increased, but manipulating balance by platform movements had no effect on stepping accuracy. However, manipulating balance delayed step onsets,



Figure 16: Experimental setup. The subject is standing on a movable platform and a lighted area appears on the floor in front of his leg, serving as a stepping cue and target.

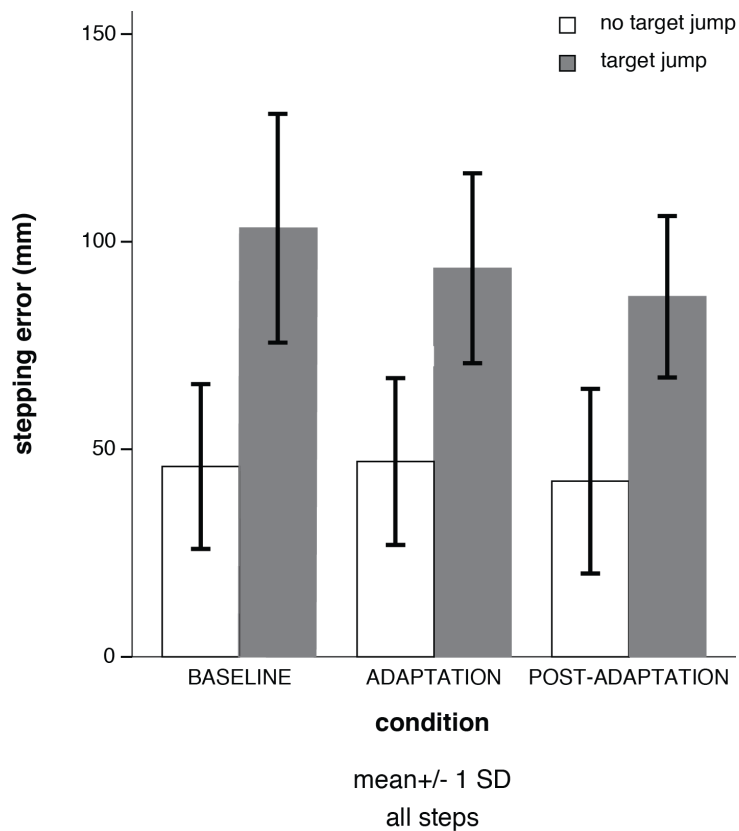


Figure 17: Stepping errors. Error bars indicate standard deviation. Statistics are given in the text.

in line with the need to adjust weight shifts prior to foot liftoff in this novel environment, and was accompanied by increased stepping errors in the first five steps. Although initially significantly perturbed, subjects quickly adapted to stepping in a novel balance environment. Analyses of weight shifting and adaptation rates of weight shifting and stepping to clarify the

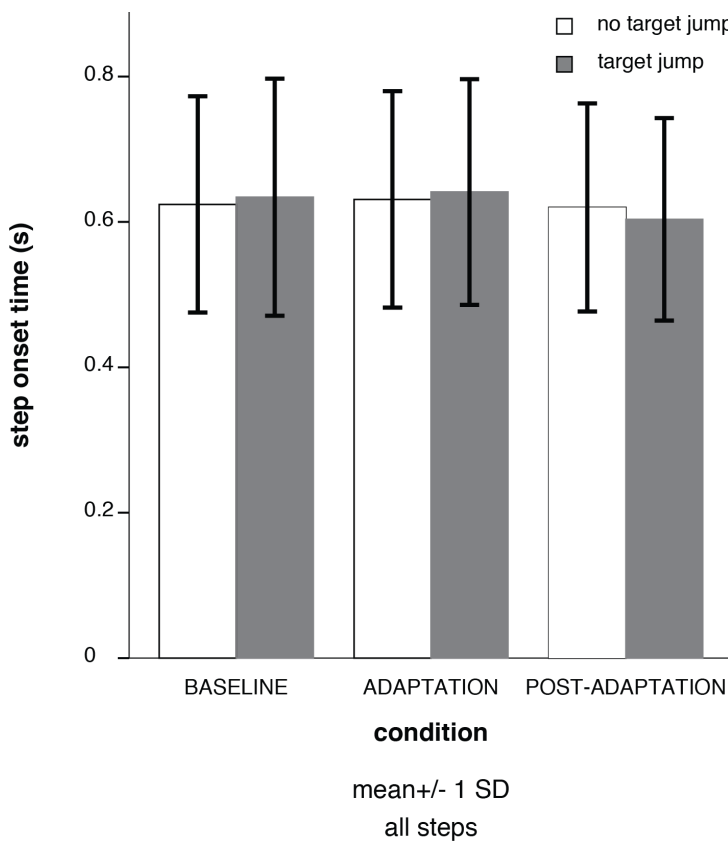


Figure 18: Step onset time (time from the cue to step to foot lift-off). Error bars indicate standard deviation. Statistics are given in the text.

underlying mechanisms are pending.

### **Investigating balance in quiet standing on a real-time movable platform system**

We investigated the effect of our newly developed real-time platform perturbation system on postural sway.

Fourteen healthy young adults stood quietly on top of a movable platform in four conditions: with their eyes open (EO), eyes closed (EC), with their eyes open and performing a memory task (memory), with their eyes open and performing an inhibitory Stroop task (Stroop). Each condition lasted for 4 minutes and we discarded the first and last 25 seconds in the data analysis. The inhibitory Stroop task required subjects to respond to the words 'high' or 'low' (in Slovenian language) delivered through headphones with an interstimulus delay of 2s. The subjects had to respond by verbalizing the pitch (and not the word) they heard. The stimuli were delivered and recorded through headphones and a microphone, which subjects wore in all conditions. The memory task required the subjects to look at a computer screen on which words appeared with an interstimulus delay of 4s. Subjects were to remember as many words as possible and their memory was checked after the condition was completed. Each of the experimental conditions was performed twice: with the platform off or with the platform moving in line with the subjects center of mass (COM) movements. The COM movements were measured using a 3x1 Optotrak camera array (Northern Digital Inc., Water-

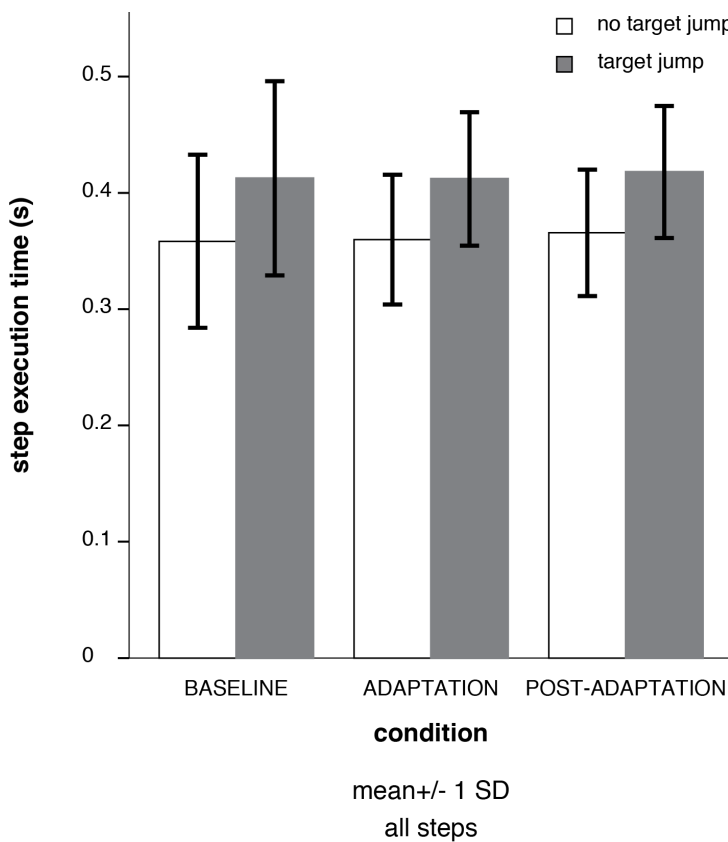


Figure 19: Step execution time (time from step onset to landing). Error bars indicate standard deviation. Statistics are given in the text.

loo, Ont., Canada), fed into a real-time computer. The real-time computer copied the COM displacements in real time into platform perturbations.

Kinematics of the COM position were high pass filtered using a second-order zero-lag Butterworth filter with a cutoff frequency of 0.1 Hz and then low pass filtered using a second-order zero-lag Butterworth filter with a cutoff frequency of 5 Hz. Outcome measures include standard deviation of the COM displacement (SD) and the range of COM displacement calculated as the difference between the 95th and 5th percentile of COM displacement, both relative to the platform movement (i.e., reflecting postural sway). Data processing was performed using MATLAB 2015b (Mathworks, Natick, MA, USA). A two-way repeated measures ANOVA with condition (EO, EC, memory, Stroop) and platform (on, off) was performed using SPSS Statistics 20 (IBM, Chicago, IL, USA), with a level of statistical significance set to  $\alpha = 0.05$ . Range data were log-transformed to conform to normality.

SD of COM displacement (mean  $\pm$  std. error of the mean) was smaller when the platform was off ( $0.47 \pm 0.05$  EO,  $0.58 \pm 0.07$  EC,  $1.00 \pm 0.19$  memory,  $1.28 \pm 0.38$  Stroop), compared to on ( $0.97 \pm 0.16$  EO,  $2.05 \pm 0.68$  EC,  $2.22 \pm 0.52$  memory,  $2.57 \pm 0.91$  Stroop). We found a statistically significant effect of platform ( $p = 0.009$ ) on the COM range (Figure 20).

Range of COM displacement (mean  $\pm$  std. error of the mean) was smaller when the platform was off ( $1.35 \pm 0.14$  EO,  $1.57 \pm 0.17$  EC,  $2.64 \pm 0.53$  memory,  $2.22 \pm 0.34$  Stroop), compared to on ( $2.71 \pm 0.24$  EO,  $4.57 \pm 0.59$  EC,  $6.92 \pm 1.65$  memory,  $6.13 \pm 1.55$  Stroop). We

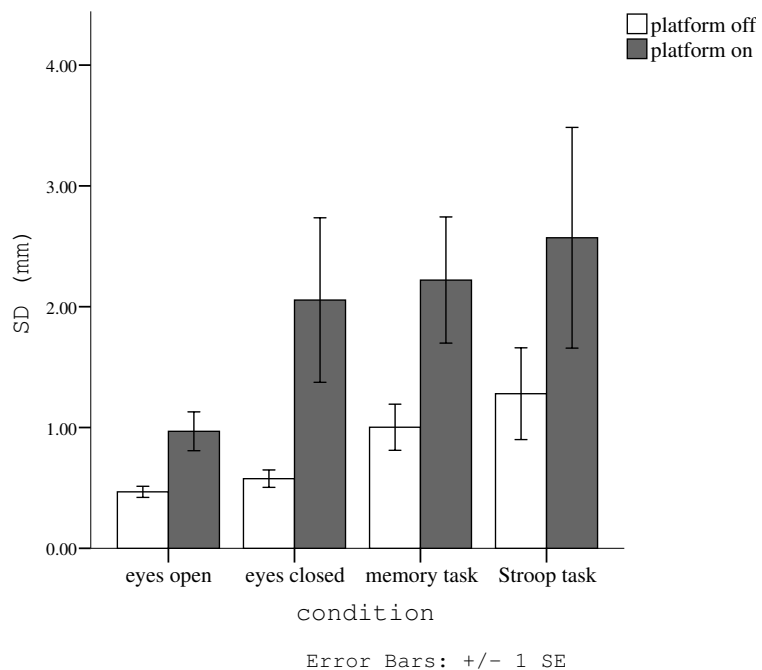


Figure 20: SD of the COM displacement (mm).

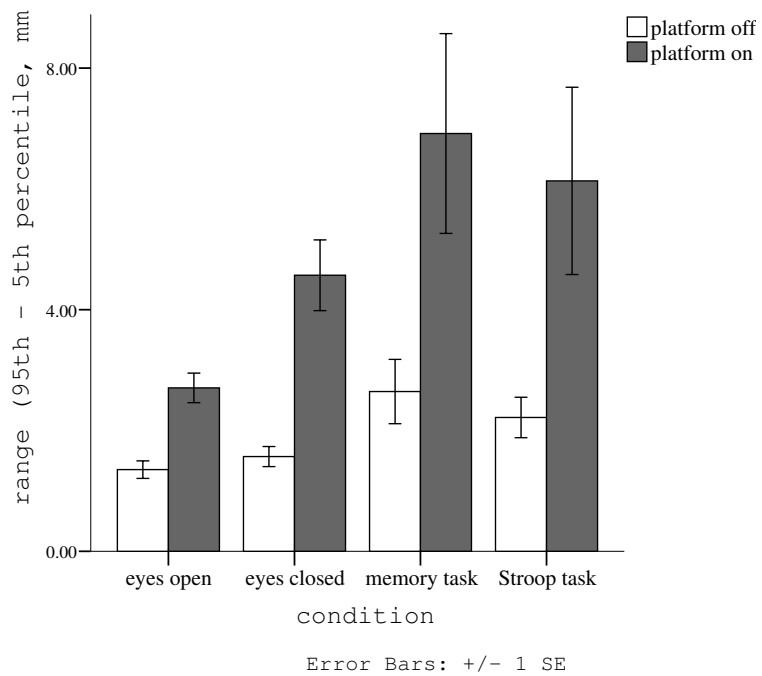


Figure 21: Range of the COM displacement (mm).

found a statistically significant effect of condition ( $p = 0.011$ ) and platform ( $p < 0.001$ ) on the COM range (Figure 21).

These data are being analyzed further and we expect them to result in at least one journal publication and a BSc thesis.

**Resources** Overall, the use of resources within WP2 was in accordance to the plans. There was an increase in the amount of PM for JSI due to the fact that we hired PhD students instead of a more efficient post-doc.

WP2 person months	IIT	TUD	UPMC	UB	JSI	INRIA
Year 1	-	-	0.28	2.64	18.80	-
Year 2	-	3.00	0.48	7.67	21.85	-
Year 3	-	1.00	1.20	13.88	21.69	0.52
Year 4	-	3.00	0.75	21.50	20.00	1.00
Partial	?	?	?	?	?	?
Overall	-	4.00	1.00	45.00	55.00	1.00

**Deviations from workplan** No significant deviations.

**3.3.2.3 Work package 3 progress** The progress for each task are described hereafter.

#### 3.3.2.3.1 Solving the local control problem (T3.3) (IIT: xxPM, UPMC: 3PM)

During the fourth year, some improvements both in terms of parametrization and in terms of generic implementation have been brought to the whole-body control problem solving methods developed in CoDyCo.

- Joint limit avoidance using an exogenous state description

During year 4, IIT proposed a control laws ensuring the stabilization of a time-varying desired joint trajectory and joint limit avoidance (see Fig. 22 for an illustration of the limits on the leg) in the case of fully-actuated manipulators. The key idea is to perform a parametrization of the feasible joint motion space in terms of exogenous states  $\xi$ , in the form of  $q(\xi) := \delta \tanh(\xi) + q_0$ , where  $q$  is the joint position,  $\delta$  the range of feasible motion and  $q_0$  its middle value. It follows that the control of the exogenous states allows for joint limit avoidance. One of the main outcomes of this work is that position terms in control laws are replaced by parametrized terms. Stability and convergence of time-varying reference trajectories obtained with the proposed method were demonstrated to be in the sense of Lyapunov. The introduced control laws were verified by carrying out experiments on two degrees-of-freedom of the torque-controlled iCub. This work led to a publication in Humanoid s 2016 [18].

- Whole-body controller implementation

As part of both WP1 and WP3, UPMC has pursued the generic implementation of an optimisation based whole-body controller named OCRA. See section 3.3.2.1) for more details and <https://github.com/ocra-recipes> and <https://ocra-recipes.github.io/web> for online resources.

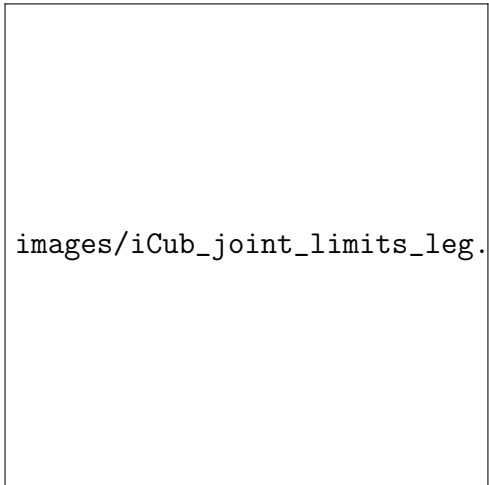


Figure 22: iCub leg setup used for the experiments. The red circles identify the hip and knee joints, while the white marks indicate joint limits. The green arrow shows the external force applied during experiments.

**3.3.2.3.2 Bootstrapping and validating the control approach in rigid world and compliant cases (T3.4) (TUD: 3.6PM, UPMC: 5.51PM, UB: xxPM, JSI: 1 PM, INRIA: 1.98PM)** Over the fourth year, the bootstrapping of the whole-body control approach developed in CoDyCo has mostly been pursued in two directions. The first one is related to the learning of the dynamics for physical interactions. The second one is related to the adaptation of tasks and their proper activation for successful whole-body motions in contact.

- **Learning torque control**

TUD and INRIA, in collaboration with WP4, continued the collaboration on the topic of learning torque control in presence of multiple contacts, exploiting the force/torque and tactile sensors of iCub. Machine learning techniques were used to directly learn the mapping from both skin and the joint state to torques, using mixtures of contact models. Recently, the model was improved for torque control by addressing critical issues in learning from high-dimensional inputs, such as the artificial skin. It was demonstrated that it is possible to considerably reduce the dimensionality of the skin data preserving the information content of the contact position by using stacked auto encoders. A journal paper is currently in preparation. This technique will allow improving torque control in presence of multiple contacts (rigid and/or soft). This work is part of the PhD thesis work of Roberto Calandra on “Bayesian Modeling for Optimization and Control in Robotics” [19].

- **Learning compliant contact models for interaction with non rigid environment**

As a part of T3.4, UB and TUD worked on developing a method to realize desired contact normal forces between a robot’s end-effector and its compliant environment. By using contact models, desired contact forces are converted to desired deformations of compliant surfaces.

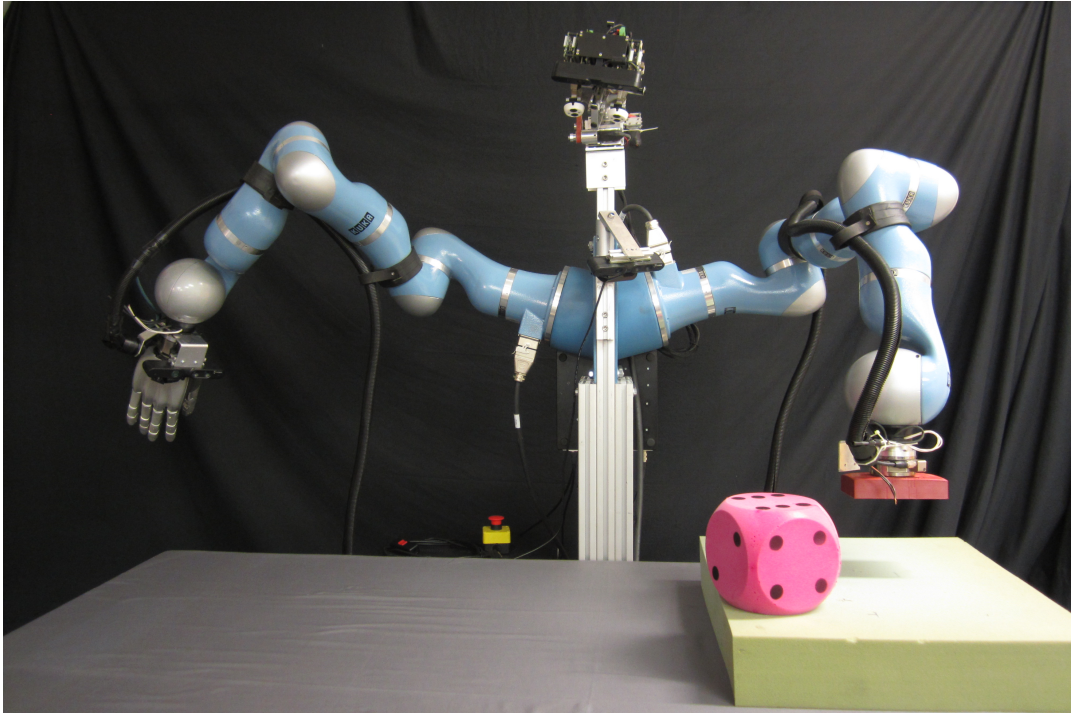


Figure 23: KUKA LWR IV arms with two soft surfaces used in our experiments.

Therefore, the problem of controlling compliant contact normal forces becomes the problem of controlling surface deformations. To study the performance of the proposed method in practice, a series of experiments, including identification and control experiments, were performed with a LWR KUKA manipulator. During the identification experiments, we estimated the contact models between the robot's end-effector and two soft surfaces using least-squared linear regression algorithm. In control experiments, by using the estimated models, we controlled the robot's motion in order to achieve various desired contact normal forces for each surface. We also studied the effects of updating model parameters during control experiments using an online estimation method. The experiment results showed that desired forces can be achieved with some errors while using the estimated model from identification experiments. These errors are decreased substantially by online adaptation of the contact model parameters during control experiments.

- **Learning soft priorities**

INRIA also designed a multi-task prioritized controller with soft task priorities. The controller was first designed in [20] and applied to classical manipulators. In [21] it was extended for whole-body movements. In the latter work, it was used to generate safe whole-body behaviors for iCub, reaching multiple goals and avoiding obstacles, with the guarantee that the generated behaviors were not violating the constraints of the platform. A software controller for iCub has been prototyped in Matlab then in C++.

- **Task compatibility optimization**

As part of both WP4 and WP3, UPMC has worked on improving its approach for task compatibility optimization. Modern control architectures employ multiple levels of control in order to decouple complex behaviors into manageable control problems. At the lowest level is reactive whole-body control, where joints torques are calculated at high frequency ( $\sim 1\text{kHz}$ ) given one or more tasks [22]. As presented in Deliverable 3.2 [23], the control problem can be written as a constrained convex optimization, where the objective function is a combination of task errors, and the constraints are the equations of motion, articulation and actuation limits, and contacts [24, 25, 26]. Task errors are calculated as the difference between the current task state and its reference value. This reference value comes from the next level of task servoing. At this level, closed loop controllers are used to servo task trajectories using state feedback (PID) or Model Predictive Control (MPC) schemes at frequencies between 100Hz and 10Hz [27], [28], [29]. These task trajectories are provided by higher-level open-loop planning which takes seconds to minutes, and generally combines operator expertise and automated planning algorithms [30, 31]. This control hierarchy of planning, servoing, and whole-body control is presented in Fig. 24.

Because each level in the control hierarchy is agnostic of the others by design, there is no guarantee that the planned task trajectories will be executed properly by the lower control layers [32, 33]. Furthermore, even though specific contexts such as non rigid contacts may be accounted for as described in Deliverable 3.2 [23], tasks may conflict with one another or be infeasible with the system constraints [34, 35]. The end result is typically unstable or undesirable whole-body behaviors, and these tasks can be qualified as *incompatible*. Prioritization techniques presented in Deliverable 3.2 [23] use weighted sums[24, 26], hierarchies [25, 36, 37] or a mix of both [38, 39] to manage task incompatibilities at the whole-body control level, but are difficult to tune and only hide the problem. Moreover, tasks incompatibilities may be temporal and change over the course of the movement so applying static priorities may be overly restrictive. While the works presented in Deliverable 4.3 [40] provide very powerful tools to reactively adapt priorities [41], learn proper prioritizations [20, 21] or derive them from demonstrations [42], it seems obvious that well designed tasks should not need to be prioritized.

Given that it is the task reference values which generate the incompatible control optima, an alternative to prioritization tuning is to modify the task trajectories supplied by planning and make them compatible as initially suggested in [43]. To do so, a feedback loop must be implemented, which measures the errors induced by incompatibilities and changes the task trajectories to reduce them. It should also take into account the servoing and whole-body control levels with all of their parameters, as well as the robot's dynamics and environment. Given the complexity of the proposed feedback loop, one solution is to use model-free Reinforcement Learning (RL) techniques to modify the trajectories through trial and error by minimizing some cost function using Black-Box Optimization (BBO) solvers [44].

The objective of the proposed approach is to establish the task compatibility optimization loop, shown on the left in Fig. 24, by iteratively improving task trajectories using RL. To do so, tasks trajectories are parameterized providing variables with which they can be modified. A generic task compatibility cost has been developed from simple principles which measures the incompatibility between one or more tasks and the robot's constraints. Using two common

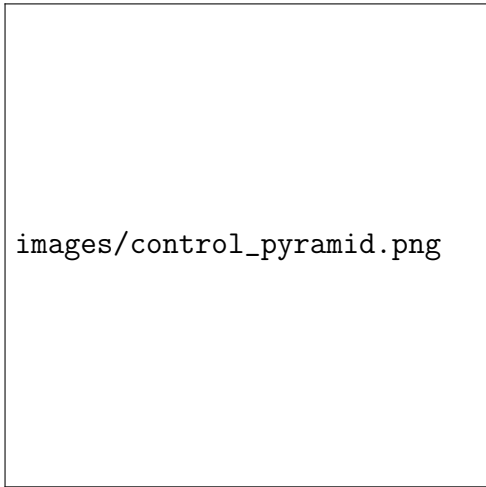


Figure 24: A modern control hierarchy for highly redundant robotic systems, e.g. humanoid robots. At the lowest level is whole-body control, which determines the torques needed to accomplish a set of tasks. At the intermediate level, these tasks are controlled by the servoing/MPC level where task trajectory errors are compensated using state feedback. Finally the task trajectories are provided by high-level planning, which is usually a combination of operator expertise and automated planning. Each of these levels operates independently from one another and a feedback mechanism is needed to measure and compensate for tasks which are not executed as planned. This is the role of the Task Compatibility Optimization loop proposed in this work.

BBO solvers, this compatibility cost can be minimized by optimizing the task trajectory parameters. This task compatibility optimization has been tested on two typical multi-task scenarios. In the first scenario the relatively banal chore of reaching while balancing has been studied. While seemingly simple, reaching is a key ingredient in robot autonomy, which often requires parameter and gain tuning before done reliably. A performance comparison of two BBO solvers for this experiment has been performed to illustrate the generality of the framework. The second experiment explores the dynamically complex activity of moving from sitting to standing. This motion requires contact breaking and potentially unstable dynamic equilibrium to succeed. In both experiments a Center of Mass (CoM) task is used to maintain balance, and its trajectory is optimized to minimize the task compatibility cost. Through these two completely different motion scenarios, the proposed generic task compatibility optimization loop has shown to dramatically improve task achievement, without ever touching the low-level control parameters. These results extend the contributions [45] and [46] both in terms of achieved performances and computational efficiency. This work and its potential use for the final demonstration are described with details in [47] and was submitted for presentation at a robotics journal [48].

- **Model Predictive stepping for robust balance**

As a part of both WP1 (see section 3.3.2.1 for a list of associated software resources) and WP3, the predictive approach initially developed by A. Ibanez [1] to preview the duration and placement of coplanar contacts has been implemented in the form of a client for OCRA using the iCub humanoid robot. Within a model-predictive control framework, the problem

is formulated as a linearly constrained mixed-integer quadratic program (MIQP) which allows the determination over a preview horizon, of the optimal changes in the base of support of the robot with compatible CoM behaviour, subject to multiple constraints, while maximising balance and performance of a walking activity.

### 3.3.2.3.3 Extra results in WP2/WP3: UPMC and JSI collaboration

- **Adapting a reaching controller using the Speed-Accuracy trade-off**

As part of both WP2 and WP3, JSI, together with UPMC, continued the computational study where they try to describe the trade-off between the speed of motion, its accuracy and the muscular cost associated with the motion. They implemented a state-of-the-art deep reinforcement learning algorithm (DDPG) that is based on a deterministic policy gradient approach. DDPG allows more sample efficient learning, but is hard to tune in the context of a simulated reaching controller. They implemented the computations on the JSI cluster in Slovenia. Computations are currently running and the analyses remain to be performed.

**3.3.2.3.4 Deviations from workplan** The PM expenses for WP3 after one year of project are globally conform to the planned one.

### 3.3.2.3.5 Resources

WP3 person months	IIT	TUD	UPMC	UB	JSI	INRIA
Year 1	9.90	4.60	15.15	-	-	-
Year 2	-	10.5	14.67	1.85	1.00	4.14
Year 3	-	9.65	8.79	1.63	2.00	4.03
Year 4	?	3.6	8.51	?	1.00	1.98
Overall	?	28.35	47.12	?	4.00	10.15
Planned	9.00	24.00	43.5	10.00	4.00	10.50

**Deviations from workplan** No major deviation from the workplan was observed.

**3.3.2.4 Work package 4 progress** The progress for each task are described hereafter.

**3.3.2.4.1 Learning the Prioritization of Tasks (T4.4) (TUD: 4PM)** TUD continued its research on learning task prioritizations from human demonstrations using probabilistic models. This work is currently under review and a draft of the paper was added to Deliverable D4.3 in Section 5. Here is a short summary of the approach.

Movement prioritization is a common approach to combine controllers of different tasks for redundant robots. Each task is assigned a priority, where either strict or 'soft' priorities can be used. While movement prioritization is an important concept in the control of whole body movements, it has been less considered in learning-based approaches, where prioritization allows us to learn different tasks for different end-effectors, and subsequently reproduce an

arbitrary, unseen combination of these tasks. This paper combines Bayesian task prioritization, a 'soft' prioritization technique, with probabilistic movement primitives to prioritize full motion sequences. Probabilistic movement primitives can encode distributions of movements over full motion sequences and provide control laws to exactly follow these distributions. The probabilistic formulation allows for a natural application of Bayesian task prioritization. We demonstrate how the 'soft' priorities can be obtained from imitation learning and that our prioritized learning architecture can reproduce unseen task-combinations. Moreover, we require less data to learn a combination of tasks than the traditional approach that directly models each task in joint space. We evaluate our approach on reaching movements under constraints with a redundant bi-manual planar robot and the humanoid robot iCub.

**3.3.2.4.2 Learning the Prioritization of Tasks (T4.4) (INRIA: 4.02PM)** INRIA continued its research on automatically learning soft task priorities (or task weights) using stochastic optimization algorithms. The research is presented in Deliverable D4.3.

The motivation for the work was to provide an automatic way of determining the temporal profile of the soft task priorities, that are classically manually tuned by experts. When done manually, the critical issue is to define the task transitions, i.e., to define when a task becomes "less important" and its weight diminishes, and viceversa.

In a first paper [49], in collaboration with TUD, we investigated how to learn the temporal profile of the soft task priorities (or task weights) in a reinforcement learning scenario. We represented the soft task priorities with parametrized weight functions, and used CMA-ES (Covariance Matrix Adaptation Evolution Strategy, a state-of-the-art black-box stochastic optimization algorithm) to optimize their parameters. We showed on a simulated and real robot manipulators that our method was able to obtain better performing solutions than the classic hand-tuned Generalized Hierarchical Controller (developed in WP3).

In a second paper [21] we focused on learning soft task priorities while guaranteeing that the generated behaviors are "safe", i.e., that they never violate any of the constraints of the robot and of the system. Indeed, CMA-ES was chosen because of its good exploration properties and ease of use (very few parameters to tune), however it does not take into account constraints violations during the exploration. In [49], the solutions that were not feasible were simply discarded. In [21] we investigated constrained stochastic optimization algorithms, focusing on three variants of CMA-ES: CMA-ES with vanilla constraints, CMA-ES with adaptive constraints and (1+1)-CMA-ES with covariance constrained adaptation. We compared the three algorithms on different benchmarks: classical constrained optimization problems with known solutions and two constrained robotics problems of our design. We found that the third method satisfies our requirements, specifically it always leads to solutions that never violate constraints. We showed the effectiveness of the approach by generating safe whole-body behaviors of iCubNancy01.

**3.3.2.4.3 Task compatibility optimization (T4.4) (UPMC: 1.87PM)** As part of WP4 and WP3, UPMC has worked on improving its approach for task compatibility optimization. Indeed, highly redundant robots, such as humanoids, can execute multiple simultaneous tasks allowing them to perform complex whole-body behaviors. Unfortunately, tasks are generally planned without close consideration for the underlying controller being used, or the other tasks being executed. Because of this, tasks are often incompatible with one another

and/or the system constraints, and cannot always be accomplished simultaneously. These incompatibilities can be managed using prioritization and gains, but tuning them is tedious. In this work, an alternative approach is taken and a task compatibility optimization loop which automatically improves task compatibility by modifying their trajectories using reinforcement learning is developed. To do so, the tasks are iteratively optimized by minimizing a compatibility cost, which measures the compatibility between one or more tasks, and the system constraints. Using two common scenarios, It is shown that task compatibility optimization results in whole-body behaviors which better match the original intent of the task combination without the need for manual tuning of task/controller parameters, heuristics, or re-planning. These results extend the contributions [45] and [46] both in terms of achieved performances and computational efficiency. This work is described in [47] and was submitted for presentation at a robotics journal [48].

## Resources

WP4 person months	IIT	TUD	UPMC	UB	JSI	INRIA
Year 1	-	8.00	2.22	-	-	-
Year 2	6.04	21.70	1.69	2.15	3.00	2.01
Year 3	9.79	12.00	0.74	1.68	3.00	3.30
Year 4	?	4	?	?	4.00	4.02
Partial	?	45.7	?	?	?	?
Overall	30.00	38.00	9.00	12.00	10.00	9.00

**Deviations from workplan** No deviations.

**3.3.2.5 Work package 5 progress** The activities in WP5 are divided into four tasks corresponding to the four years project duration. As a result, during the fourth year CoDyCo results concentrate on T5.4. The main result consist in the implementation of the validation scenario consisting of the balancing with the help of a caregiver. The main scientific contribution is described here [50].

**3.3.2.5.1 Scenario 4: learning how to stand up with the help of a human caregiver (T5.4)** The main contributions to T5.4 have been presented in “Validation scenario 4: learning how to stand up with the help of a human caregiver” which discusses the technical implementation of the fourth year validation scenario (see <https://github.com/robotology-playground/codyco-deliverables/tree/master/D5.4/pdf>). The software developed for the scenario implementation is released with an open-source license and distributed through github (<https://github.com/robotology/codyco>).

### CoM Dynamic Manipulability for the iCub in a Sitting Configuration

In this calculations, it is assumed that the robot is in a sitting configuration with joint angles mentioned in Table 2. Shoulder pitch angle ( $\alpha$ ) and elbow angle ( $\beta$ ) are the two variables which are used to maximize the CoM dynamic manipulability in a desired direction.

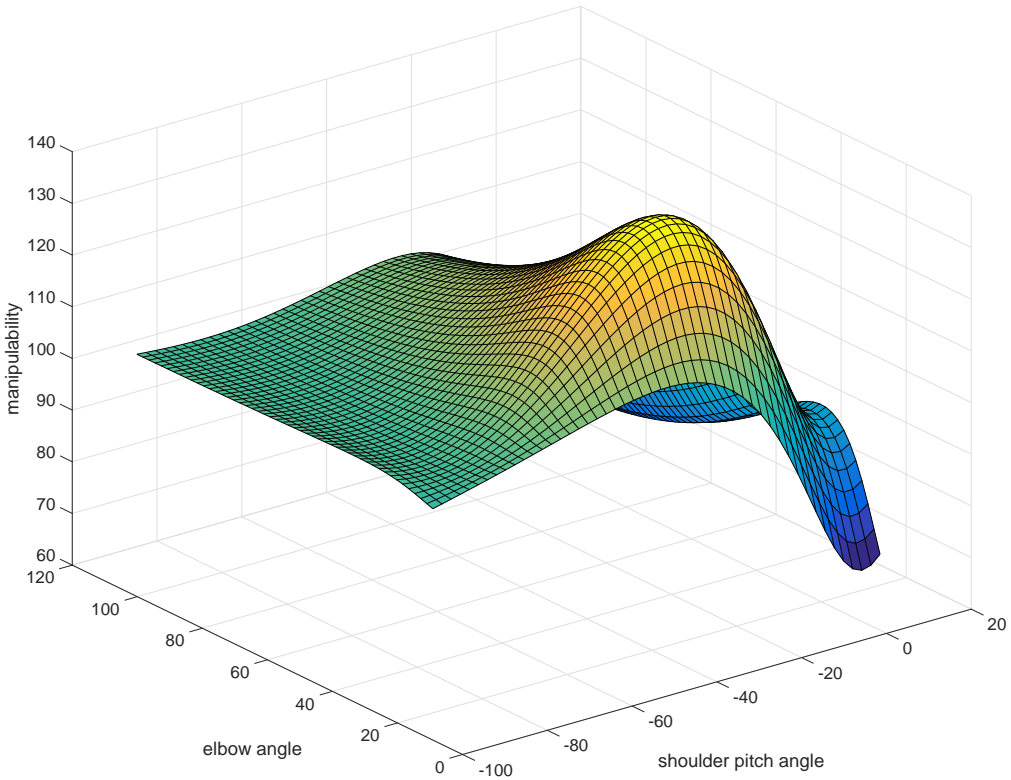


Figure 25: CoM dynamic manipulability with respect to arm configuration.

The desired direction of the CoM movement in the beginning of the motion is horizontal. The maximum joint torques are assumed to be 40N.m. for the legs and 20N.m. for the arms.

Table 2: iCub joint angles in a sitting configuration. Angles are in degrees.

hip pitch	91	shoulder roll	12	torso pitch	-5
hip roll	12	shoulder yaw	80	torso roll	0
hip yaw	0	wrist pronos	0	torso yaw	0
knee	-104	wrist pitch	0	neck pitch	0
ankle pitch	-12	wrist yaw	0	neck roll	0
ankle roll	0			neck yaw	0.5

The CoM dynamic manipulability for different arm configurations (i.e. different  $\alpha$  and  $\beta$ ) is shown in Figure 25. The maximum manipulability is at  $\alpha = -29^\circ$  and  $\beta = 32^\circ$ . Figures 26 and 27 show CoM manipulability with respect to the shoulder angle and the elbow angle, respectively. As it can be seen in these figures, in case the optimum values are not feasible, best values for the shoulder angle value is between  $-20^\circ$  to  $-40^\circ$  and for the elbow angle is about  $30^\circ$ . Figures 28 shows the iCub's configurations when the arms angles are in their optimum values. Figure 29 shows the iCub's configuration when  $\alpha = -40^\circ$  and  $\beta = 32^\circ$ . In this case, the manipulability is decreased by %3.

### 3.3.2.5.2 Deviations from workplan No deviations.

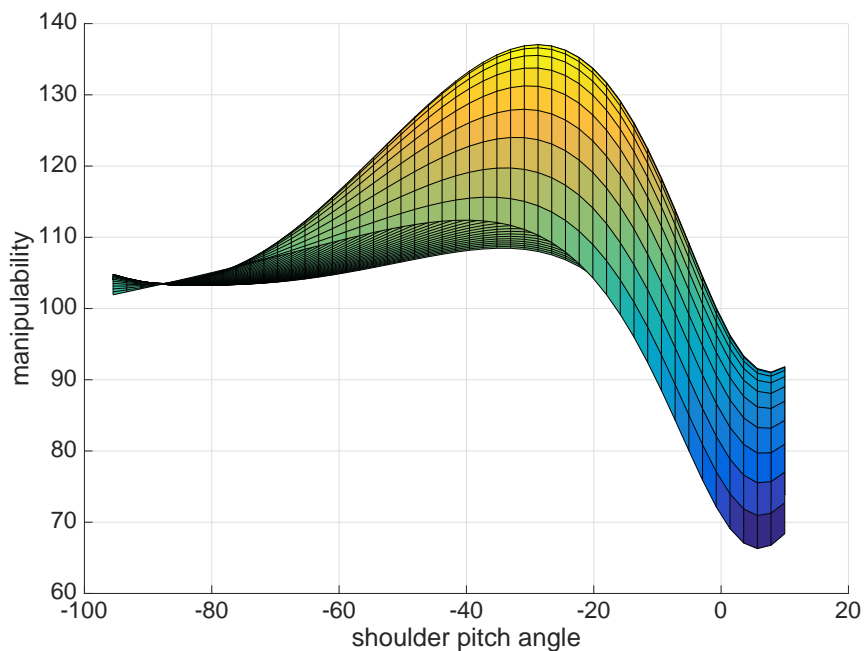


Figure 26: CoM dynamic manipulability with respect to shoulder pitch angle.

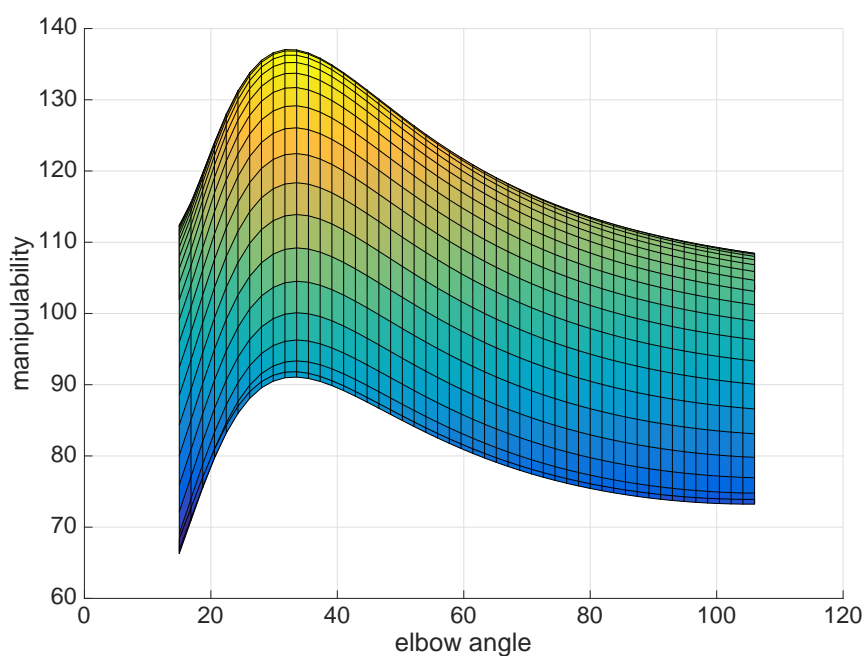


Figure 27: CoM dynamic manipulability with respect to elbow angle.

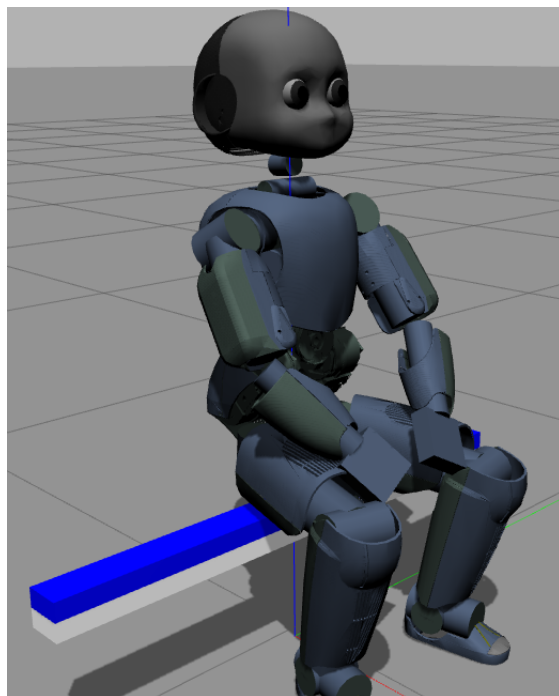


Figure 28: iCub in optimum sitting configuration.

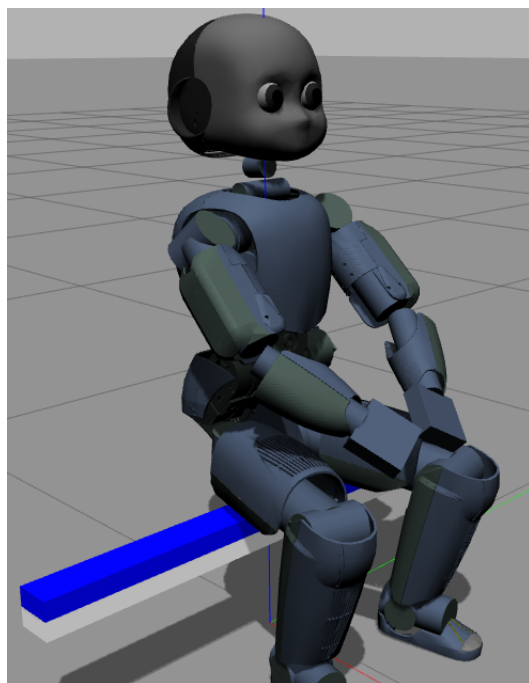


Figure 29: iCub in near-optimum sitting configuration.

**Resources** Resources were used with no difference with respect to what planned.

WP5 person months	IIT	TUD	UPMC	UB	JSI	INRIA
Year 1	2.00	-	0.31	-	-	-
Year 2	12.00	0.85	0.05	-	-	-
Year 3	13.06	2.00	0.14	1.44	-	0.52
Year 4	?	?	?	?	?	?
Partial	?	?	?	?	?	?
Overall	48.00	5.00	2.50	-	-	1.50

**Deviations from workplan** No significant deviations from the workplan. The validation scenarios will include all the theoretical and technological challenges detailed in the original plan.

**3.3.2.6 Work package 6 progress** Activities within work package 6 achieved the expected results both in terms of administrative activities and management activities. As a major result, the software repository was consolidated thanks to the versioning tool (git) and social coding website (<https://github.com>).

**3.3.2.6.1 Administrative coordination (T6.1)** Administration was successfully coordinated by Chiara Andreoli at IIT. The major activity concerned an amendment that the CoDyCo consortium asked the main reason being the fact that Serena Ivaldi, initially hired by UPMC, lately moved to UPMC and finally integrated in the consortium with INRIA. Part of the administrative coordination activities were also conducted during the mid-year meeting: Nancy, November 22nd, 2016. Details on the meetings can be found in the CoDyCo website (<http://www.codyco.eu>).

**3.3.2.6.2 Software repository implementation (T6.2)** A github software repository was set up <https://github.com/robotology/codyco> and the contribution from the different developers can be directly checked in the website.

**Resources** Resources were used as follows.

WP6 person months	IIT	TUD	UPMC	UB	JSI	INRIA
Year 1	1.46	-	0.25	-	-	-
Year 2	1.50	-	0.31	-	-	-
Year 3	1.51	1.00	0.19	-	0.44	-
Year 4	?	?	?	?	0.54	?
Partial	?	?	?	?	?	?
Overall	5.00	1.00	1.00	0.60	1.00	-

**Deviations from workplan** No significant deviations.

**3.3.2.7 Work package 7 progress** Dissemination and exploitation activities included the participation to international events addressed to both commercial and academic institutions.

**3.3.2.7.1 Dissemination activities towards academia, industry, and other users**

**(T7.1)** The explicit goal of T7.1 for the fourth year was to ...

We achieved the following results ...

**3.3.2.7.2 Exploitation plan (T7.2)** The explicit goal of T7.2 for the fourth year was to ...

We achieved the following results ...

**3.3.2.7.3 Management of IPR (T7.3)** The explicit goal of T7.3 for the fourth year was to ...

We achieved the following results ...

**3.3.2.7.4 Dissemination of a database of human motion with contacts (T7.4)**

The explicit goal of T7.4 for the fourth year was to ...

We achieved the following results ...

**Resources** Resources were used as follows.

WP7 person months	IIT	TUD	UPMC	UB	JSI	INRIA
Year 1	1.00	-	0.40	-	-	-
Year 2	-	-	0.13	-	-	0.91
Year 3	1.00	-	0.11	-	-	-
Year 4	?	?	?	?	1.00	?
Partial	?	?	?	?	?	?
Overall	3.00	1.00	1.00	1.00	1.00	1.00

**Deviations from workplan** No significant deviations.

## 3.4 Deliverables and milestones tables

### 3.4.1 Deliverables (excluding the periodic and final reports)

### 3.4.2 Milestones

Del. no.	Deliverable name	WP	Type	Date	Responsible	Person Month
D1.2	Software for controlling of balancing and reaching with multiple contacts.	1	SW	M24	UB	16
D3.1	Local solver in rigid-world cases.	3	R	M24	UPMC	18
D4.2	Learning of tasks with multiple contacts by imitation and reinforcement learning.	4	R	M24	TUD	30
D5.2	Validation scenario2: balancing on feet while performing goal directed actions.	5	R	M24	IIT	13

R = Report, P = Prototype, D = Demonstrator, SW = Software, O = Other

Milestone number	Milestone name	Work package(s) involved	Expected date <sup>1</sup>	Leader	Means of verification
MS.2	Validation scenario2: balancing on feet while performing goal directed actions	MS.1 T1.3 T1.5 T4.3 T5.2	M24	IIT	- The iCub successfully reaches an object while exploiting multiple contacts

## References

- [1] A. Ibanez, "Emergence of complex behaviors from coordinated predictive control in humanoid robotics," Ph.D. dissertation, Université Pierre et Marie Curie Paris VI, Sep.

2015. [Online]. Available: <http://hal.upmc.fr/tel-01308723>
- [2] R. D. Roberts and G. W. Humphreys, "The role of somatotopy and body posture in the integration of texture across the fingers," *Psychological Science*, 2010.
- [3] R. D. Roberts, "Roughness perception across the hands," *Attention, Perception, & Psychophysics*, vol. 75, no. 6, pp. 1306–1317, 2013.
- [4] M. Hollins and S. R. Risner, "Evidence for the duplex theory of tactile texture perception," *Perception & Psychophysics*, vol. 62, no. 4, pp. 695–705, 2000. [Online]. Available: <http://dx.doi.org/10.3758/BF03206916>
- [5] J. M. Yau, P. Celnik, S. S. Hsiao, and J. E. Desmond, "Feeling better separate pathways for targeted enhancement of spatial and temporal touch," *Psychological science*, p. 0956797613511467, 2014.
- [6] M. Darainy, A. A. G. Mattar, and D. J. Ostry, "Effects of human arm impedance on dynamics learning and generalization," *Journal of Neurophysiology*, vol. 101(6), pp. 3158–3168, 2008.
- [7] F. Mussa-Ivaldi, N. Hogan, and E. Bizzi, "Neural, mechanical, and geometric factors subserving arm posture in humans," *Journal of Neuroscience*, vol. 5, no. 10, pp. 2732–2743, 1985. [Online]. Available: <http://www.jneurosci.org/content/5/10/2732>
- [8] E. Burdet, R. Osu, D. W. Franklin, T. E. Milner, and M. Kawato, "The central nervous system stabilizes unstable dynamics by learning optimal impedance," *Nature*, vol. 414, no. 6862, pp. 446–449, 2001.
- [9] T. Tsuji, Y. Takeda, and Y. Tanaka, "Analysis of mechanical impedance in human arm movements using a virtual tennis system," *Biological Cybernetics*, vol. 91, no. 5, pp. 295–305, 2004. [Online]. Available: <http://dx.doi.org/10.1007/s00422-004-0515-1>
- [10] K. P. Tee, E. Burdet, C.-M. Chew, and T. E. Milner, "A model of force and impedance in human arm movements," *Biological cybernetics*, vol. 90, no. 5, pp. 368–375, 2004.
- [11] S. Ivaldi, S. Lefort, J. Peters, M. Chetouani, J. Provasi, and E. Zibetti, "Towards engagement models that consider individual factors in hri: On the relation of extroversion and negative attitude towards robots to gaze and speech during a human–robot assembly task," *International Journal of Social Robotics*, vol. 9, p. 6386, 2017.
- [12] S. M. Anzalone, G. Varni, S. Ivaldi, and M. Chetouani, "Automated prediction of extraversion during human–humanoid interaction," *International Journal of Social Robotics*, pp. 1–15, 2017.
- [13] S. R. Lord and R. C. Fitzpatrick, "Choice stepping reaction time: a composite measure of falls risk in older people." *The journals of gerontology. Series A, Biological sciences and medical sciences*, vol. 56, no. 10, pp. M627–32, oct 2001. [Online]. Available: <http://www.ncbi.nlm.nih.gov/pubmed/11584035>

- [14] R. G. Cohen, J. G. Nutt, and F. B. Horak, "Errors in postural preparation lead to increased choice reaction times for step initiation in older adults." *The journals of gerontology. Series A, Biological sciences and medical sciences*, vol. 66, no. 6, pp. 705–13, jun 2011. [Online]. Available: <http://www.ncbi.nlm.nih.gov/pubmed/21498431><http://www.ncbi.nlm.nih.gov/pmc/articles/PMC3110912/>
- [15] P. J. Sparto, S. I. Fuhrman, M. S. Redfern, J. R. Jennings, S. Perera, R. D. Nebes, and J. M. Furman, "Postural adjustment errors reveal deficits in inhibition during lateral step initiation in older adults." *Journal of neurophysiology*, vol. 109, no. 2, pp. 415–28, jan 2013. [Online]. Available: <http://www.ncbi.nlm.nih.gov/pmc/articles/PMC3545456/>{&}tool=pmcentrez{&}rendertype=abstract
- [16] M. L. Mille, M. Simoneau, and M. W. Rogers, "Postural dependence of human locomotion during gait initiation." *Journal of neurophysiology*, vol. 112, no. 12, pp. 3095–103, 2014. [Online]. Available: <http://www.ncbi.nlm.nih.gov/pubmed/25231611>
- [17] S. N. Robinovitch, F. Feldman, Y. Yang, R. Schonnop, P. M. Leung, T. Sarraf, J. Sims-Gould, and M. Loughin, "Video capture of the circumstances of falls in elderly people residing in long-term care: an observational study." *Lancet*, vol. 381, no. 9860, pp. 47–54, jan 2013. [Online]. Available: <http://www.ncbi.nlm.nih.gov/pmc/articles/PMC3540102/>{&}tool=pmcentrez{&}rendertype=abstract
- [18] M. Charbonneau, F. Nori, and D. Pucci, "On-line joint limit avoidance for torque controlled robots by joint space parametrization," in *Proceedings of the IEEE-RAS 16th International Conference on Humanoid Robots*, Cancun, Mexico, Nov. 2016, pp. 899–904.
- [19] R. Calandra, "Bayesian modeling for optimization and control in robotics," Ph.D. dissertation, TU Darmstadt, Darmstadt, Germany, 2016.
- [20] V. Modugno, G. Neumann, E. Rueckert, G. Oriolo, J. Peters, and S. Ivaldi, "Learning soft task priorities for control of redundant robots," in *IEEE International Conference on Robotics and Automation*, May 2016, pp. 221–226.
- [21] V. Modugno, U. Chervet, G. Oriolo, and S. Ivaldi, "Learning soft task priorities for safe control of humanoid robots with constrained stochastic optimization," in *Humanoid Robots (Humanoids), 2016 IEEE-RAS 16th International Conference on*. IEEE, 2016, pp. 101–108.
- [22] O. Khatib, L. Sentis, J. Park, and J. Warren, "Whole-body dynamic behavior and control of human-like robots," *International Journal of Humanoid Robotics*, vol. 1, no. 01, pp. 29–43, 2004.
- [23] M. Azzad, M. Liu, M. Mistry, F. Nori, V. Padois, D. Pucci, F. Romano, and S. Traversaro, "Codyco project, deliverable 3.2: Local solver in compliant-world cases," Sorbonne Universités, UPMC Paris 06, UMR CNRS 7222, Tech. Rep., Feb. 2016.

- [24] J. Salini, V. Padois, and P. Bidaud, "Synthesis of complex humanoid whole-body behavior: A focus on sequencing and tasks transitions," in *IEEE International Conference on Robotics and Automation*, May 2011, pp. 1283–1290.
- [25] L. Saab, O. E. Ramos, F. Keith, N. Mansard, P. Soueres, and J.-Y. Fourquet, "Dynamic whole-body motion generation under rigid contacts and other unilateral constraints," *IEEE Transactions on Robotics*, vol. 29, no. 2, pp. 346–362, 2013.
- [26] K. Bouyarmane and A. Kheddar, "Using a multi-objective controller to synthesize simulated humanoid robot motion with changing contact configurations," in *IEEE/RSJ International Conference on Intelligent Robots and Systems*. IEEE, 2011, pp. 4414–4419.
- [27] A. Ibanez, P. Bidaud, and V. Padois, "Emergence of humanoid walking behaviors from Mixed-Integer Model Predictive Control," in *IEEE/RSJ International Conference on Intelligent Robots and Systems*, Chicago, USA, Sept 2014, pp. 4014 – 4021.
- [28] J. Koenemann, A. D. Prete, Y. Tassa, E. Todorov, O. Stasse, M. Bennewitz, and N. Mansard, "Whole-body model-predictive control applied to the HRP-2 humanoid," in *IEEE/RSJ International Conference on Intelligent Robots and Systems*, Sept 2015, pp. 3346–3351.
- [29] N. Perrin, D. Lau, and V. Padois, "Effective Generation of Dynamically Balanced Locomotion with Multiple Non-coplanar Contacts," in *International Symposium on Robotics Research*, 2015.
- [30] K. Bouyarmane and A. Kheddar, "Humanoid robot locomotion and manipulation step planning," *Advanced Robotics*, vol. 26, no. 10, pp. 1099–1126, 2012.
- [31] Q.-C. Pham, "A general, fast, and robust implementation of the time-optimal path parameterization algorithm," *IEEE Transactions on Robotics*, vol. 30, no. 6, pp. 1533–1540, Dec 2014.
- [32] V. Padois, "Control and design of robots with tasks and constraints in mind," *Habilitation Diriger des Recherches*, Universit Pierre et Marie Curie, Paris, France, Oct. 2016. [Online]. Available: <http://hal.archives-ouvertes.fr/tel-01398868/en>
- [33] A. Ibanez, P. Bidaud, and V. Padois, "Optimization-based control approaches to humanoid balancing," in *Humanoid Robotics: a Reference*, A. Goswami and P. Vadakkepat, Eds. Springer Netherlands, 2016, accepted for publication.
- [34] K. Bouyarmane and A. Kheddar, "On Weight-Prioritized Multi-Task Control of Humanoid Robots," *IEEE Transactions on Automatic Control*, in revision 2015.
- [35] P.-B. Wieber, A. Escande, D. Dimitrov, and A. Sherikov, "Geometric and numerical aspects of redundancy," in *Geometric and Numerical Foundations of Movements*, 2017.
- [36] A. Escande, N. Mansard, and P.-B. Wieber, "Hierarchical quadratic programming: Fast online humanoid-robot motion generation," *The International Journal of Robotics Research*, vol. 33, no. 7, pp. 1006–1028, 2014.

- [37] A. Dietrich, C. Ott, and A. Albu-Schäffer, "An overview of null space projections for redundant torque-controlled robots," *The International Journal of Robotics Research*, vol. 34, no. 11, pp. 1385–1400, 2015.
- [38] M. Liu, Y. Tan, and V. Padois, "Generalized hierarchical control," *Autonomous Robots*, vol. 40, no. 1, pp. 17–31, 2016.
- [39] M. Liu, R. Lober, and V. Padois, "Whole-body hierarchical motion and force control for humanoid robots," *Autonomous Robots*, vol. 40, no. 3, pp. 493–504, 2016.
- [40] R. Lober, V. Padois, O. Sigaud, V. Modugno, G. Neumann, E. Rueckert, G. Oriolo, J. Peters, S. Ivaldi, and A. Paraschos, "Codyco project, deliverable 4.3: Learning of the prioritization policies," Technische Universität Darmstadt & Jozef Stefan Institute, Tech. Rep., Feb. 2016.
- [41] R. Lober, V. Padois, and O. Sigaud, "Variance modulated task prioritization in Whole-Body Control," in *IEEE/RSJ International Conference on Intelligent Robots and Systems*, Sept 2015, pp. 3944–3949.
- [42] A. Paraschos, J. Peters, and G. Neumann, "Probabilistic prioritization of movement primitives," 2017, under review.
- [43] R. Lober, V. Padois, and O. Sigaud, "Multiple task optimization using dynamical movement primitives for whole-body reactive control," in *IEEE-RAS International Conference on Humanoid Robots*, Nov 2014, pp. 193–198.
- [44] J. Kober, J. A. Bagnell, and J. Peters, "Reinforcement learning in robotics: A survey," *The International Journal of Robotics Research*, vol. 32, no. 11, pp. 1238–1274, 2013.
- [45] R. Lober, V. Padois, and O. Sigaud, "Multiple task optimization using dynamical movement primitives for whole-body reactive control," in *Proceedings of the IEEE-RAS International Conference on Humanoid Robots (Humanoids)*, Madrid, Spain, 2014.
- [46] ——, "Variance modulated task prioritization in whole-body control," in *Proceedings of the IEEE/RSJ International Conference on Intelligent Robots and Systems*, Hamburg, Germany, Sep 2015, pp. 3944–3949.
- [47] M. Azad, P. Bidaud, U. Chervet, A. Ibanez, S. Ivaldi, D. Lau, H. C. Lin, R. Lober, M. Misstry, V. Modugno, G. Neumann, F. Nori, G. Oriolo, V. Ortenzi, V. Padois, A. Paraschos, N. Perrin, J. Peters, D. Pucci, F. Romano, E. Rueckert, O. Sigaud, and S. Traversaro, "Codyco project, deliverable 3.3: Local solver in compliant and unforeseen cases," Sorbonne Universités, UPMC Paris 06, UMR CNRS 7222, Tech. Rep., Feb. 2017.
- [48] R. Lober, V. Padois, and O. Sigaud, "Task compatibility optimization," *IEEE Robotics and Automation Letters*, 2017, submitted.
- [49] V. Modugno, G. Neumann, E. Rueckert, G. Oriolo, J. Peters, and S. Ivaldi, "Learning soft task priorities for control of redundant robots," in *Proceedings of the International Conference on Robotics and Automation (ICRA)*, 2016.

- [50] C. Latella, N. Kuppuswamy, F. Romano, S. Traversaro, and F. Nori, "Whole-body human inverse dynamics with distributed micro-accelerometers, gyros and force sensing," *Sensors*, vol. 16, no. 5, p. 727, 2016.